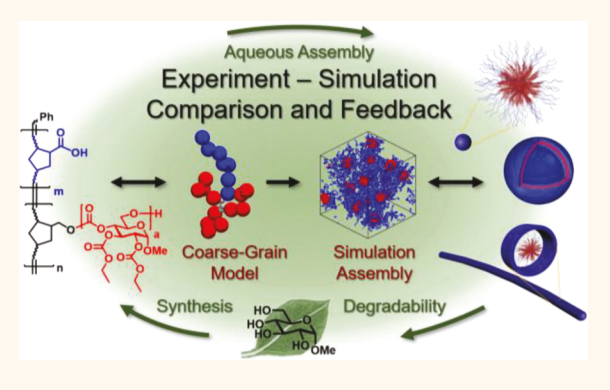


# **Experiments and Simulations of Complex** Sugar-Based Coil-Brush Block Polymer Nanoassemblies in Aqueous Solution

Mei Dong, †, Louis Michiel G. Wessels, †, Louis Lee, Lu Su, † Hai Wang, Rachel A. Letteri, Yue Song, Yen-Nan Lin, †, Yingchao Chen, Richen Li, Darrin J. Pochan, Arthi Jayaraman, \*, †, So and Karen L. Wooley\*,†6

Supporting Information

ABSTRACT: In this work, we investigated the fundamental molecular parameters that guide the supramolecular assembly of glucose-based amphiphilic coil-brush block polymers in aqueous solution and elucidated architecture-morphology relationships through experimental and simulation tools. Well-defined coilbrush polymers were synthesized through ring-opening polymerizations (ROP) of glucose carbonates to afford norbornenylfunctionalized poly(glucose carbonate) (NB-PGC) macromonomers, followed by sequential ring-opening metathesis polymerizations (ROMP) of norbornene N-hydroxysuccinimidyl (NHS) esters and the NB-PGC macromonomers. Variation of the macromonomer length and grafting through ROMP conditions allowed for a series of coil-brush polymers to be synthesized with



differences in the brush and coil dimensions, independently, where the side chain graft length and brush backbone were used to tune the brush, and the coil block length was used to vary the coil. Hydrolysis of the NHS moieties gave the amphiphilic coil-brush polymers, where the hydrophilic-hydrophobic ratios were dependent on the brush and coil relative dimensions. Experimental assembly in solution was studied and found to yield a variety of structurally dependent nanostructures. Simulations were conducted on the solution assembly of coil-brush polymers, where the polymers were represented by a coarse-grained model and the solvent was represented implicitly. There is qualitative agreement in the phase diagrams obtained from simulations and experiments, in terms of the morphologies of the assembled nanoscopic structures achieved as a function of coil-brush design parameters (e.g., brush and coil lengths, composition). The simulations further showed the chain conformations adopted by the coil-brush polymers and the packing within these assembled nanoscopic structures. This work enables the predictive design of nanostructures from this glucose-based coil brush polymer platform while providing a fundamental understanding of interactions within solution assembly of complex polymer building blocks.

KEYWORDS: coil—brush block polymers, aqueous self-assembly, coarse-grained simulation, biobased materials, phase diagrams

5147

lacktriance english effectively elf-assembly of degradable synthetic polymers, especially those with increasing topological complexity, has been studied for several decades as a powerful way to create nanostructures, and the vast amount of experimental work is now experiencing iterative interplay with guidance by theoretical and computational advances. Obtaining more complex nanostructures has long fascinated researchers at the

interface of biology, chemistry, materials science, and medicine<sup>1-4</sup> and motivated the design of amphiphilic macromolecules with degradability, e.g., polyesters, polypeptides, and

Received: November 19, 2018 Accepted: April 10, 2019 Published: April 16, 2019



Departments of Chemistry, Chemical Engineering, Materials Science & Engineering, and the Laboratory for Synthetic-Biologic Interactions, Texas A&M University, College Station, Texas 77843, United States

<sup>&</sup>lt;sup>‡</sup>Department of Chemical & Biomolecular Engineering, Colburn Laboratory, University of Delaware, Newark, Delaware 19716, United States

<sup>§</sup>Department of Materials Science and Engineering, University of Delaware, Newark, Delaware 19716, United States

College of Medicine, Texas A&M University, Bryan, Texas 77807, United States

polycarbonates, 5-13 as well as sophisticated architectures, e.g., cyclic, bottlebrush, and branched structures. 14-16 Precisely constructed brush polymers are of increasing interest, especially multifunctional bottlebrushes that are capable of supramolecular assembly into biologically active nanomaterials, due to their physicochemical properties, such as their extended backbone conformation, hindered entanglement, and feasibility as nanoscopic molecular building blocks with tunable relative concentric and lengthwise dimensions. <sup>17–20</sup> Coil–brush block polymers, also known as linear-block-brush polymers, contain both a flexible linear structure and a bulky bottlebrush structure, resulting in a wide range of compositional variables over both blocks, individually, as well as their combined twodimensional architectures. The assembly behavior of coilbrush polymers is expected to be fundamentally different from either linear or brush block polymers; the molecular parameters within their unconventional asymmetric architecture are associated with an interesting set of trade-offs between various polymer-polymer/surface/solvent interactions in the system, caused by their intrinsic imbalances. Owing to their molecular geometry, they exhibit distinct microphase separation patterns in the bulk and at interfaces and assemble into defined aggregates in solution. 21-32 Among all the characteristics, the ability of amphiphilic coil-brush polymers to selfassemble into numerous nanoscopic objects, including spherical, 33-35,23,28 hexagonal, 36 cylindrical, 37,38 vesicle, 39 lamellar morphologies, <sup>36</sup> etc., offers significant diversity in the construction of well-defined nanoscopic materials. Schmidt and co-workers have reported the synthesis and self-assembly of poly(styrene-block-((2-isobutyryloxy)ethyl methacrylate)graft-(acrylic acid)) (PS-b-(P'BEMA-g-PAA)) coil-brush block polymers that were observed to form star-like micelles in aqueous solution by scanning force microscopy.<sup>4</sup> Hadjichristidis and co-workers have studied the micellization behavior of complex comb-like block polymers containing polystyrene, polyisoprene, or polybutadiene components with various architectures. 41 Xi, Chen, and co-workers synthesized amphiphilic comb-dendronized diblock polymers composed of a hydrophobic Percec-type dendronized polystyrene block and a hydrophilic comb-like poly(ethylene oxide) grafted polymethacrylate block and obtained diverse morphologies, such as twisted string, vesicle, and large compound micelles in a mixture of methanol and tetrahydrofuran. 42 Lin and coworkers reported the synthesis and self-assembly behavior of an amphiphilic coil-brush block polymer bearing hydrophilic poly(ethylene glycol) and hydrophobic polypeptide brush segments in aqueous solution and investigated the assembly morphology as a function of brush length.<sup>4</sup>

The breadth of the types of polymers that can be designed, synthesized, and assembled experimentally has been growing, inspiring the use of theoretical and computational tools to investigate increasingly complex polymers and predict molecular features of the polymers needed to achieve nanostructures that meet the design criteria for specific applications. Theory and molecular simulations allow for systematic variation of parameters in polymer design and explanation of the molecular packing within the assembled states as a function of the polymer design; this motivates the synergistic use of theory and simulations with experiments. Simulation and theory have been used to study coil-branched architectures such as coil—dendrimer, coil—star, and coil—brush block polymer assembly in melt-like conditions 17-64 and in solution. Solution assembly of

linear-branched architectures, namely, single examples of each of the following architectures: linear-linear, linear-comb, linear-star, and linear-dendritic copolymers, have been studied by Cheng and co-workers, who used Brownian dynamics simulations to find that the critical micelle concentration increases with increased branching, while the micelle size and aggregation number decrease with increased branching.<sup>66</sup> Self-consistent field theory (SCFT) calculations have been used to investigate coil-brush block polymer micelles with a solvophobic backbone and solvophilic side chains, showing a bimodal distribution of micelles where the backbone section with grafted side chains either separates to the core—corona interface or forms part of the corona. 67 These studies indicate the ability of computational tools to systematically vary the coil-brush design parameters and study their effect on the resulting molecular packing and micellization behavior.

Herein, we report the synthesis, molecular modeling, and assembly of a series of asymmetric coil-brush block polymers containing a flexible, hydrophilic carboxylic acid coil block and a rigid, hydrophobic bottlebrush block composed of hydrolytically degradable glucose carbonate-based oligo/polymeric side chain grafts. We developed an intermediate resolution coarse-grained model to mimic the synthesized coil-brush block polymers in molecular dynamics (MD) simulations. The design of the coil-brush block polymers was followed by their assembly through a dialysis-based solvent exchange process in experiments and by directly changing the solvent quality to mimic solvent exchange in simulations. As a result, phase diagrams using both experiment and simulation were constructed, showing that the morphology depends on both the length of hydrophobic side chains and the overall hydrophilic/hydrophobic ratio, described in terms of the molar ratio of carboxylic acid units to glucose carbonate units (A/G). 69,70 The morphologies of the assembled structures as a function of coil-brush design parameters matched well between the experiments and MD simulations. We also quantified the chain packing parameters within the assembled structures in the simulations and found how the packing parameter changes with the coil-brush polymer design. This experiment-simulation work validates the coarse-grained model and provides a platform for further investigation using both simulation and experiment to explore wider design parameter space and establish design rules for assembly toward desired nanostructures. 72,73,11

# **RESULTS AND DISCUSSION**

Coil-brush block polymers were synthesized and assembled to yield core-degradable nano-objects in aqueous media with functionalizable coronas. Ring-opening polymerizations (ROP) of cyclic glucose carbonates was initiated by a norbornenefunctionalized alcohol to afford a series of norborneneterminated poly(glucose carbonate) (PGC) macromonomers, followed by sequential ring-opening metathesis polymerizations (ROMP) of a norbornenyl-functionalized N-hydroxysuccinimidyl (NHS) ester monomer and the norborneneterminated PGC macromonomers to achieve the well-defined coil-brush architecture with high grafting efficiency and tunable chemical compositions. Hydrolysis of the NHS groups generated amphiphilic coil-brush block polymers that assembled in aqueous solutions into various nanoscopic morphologies. Several compositional parameters, such as hydrophilic(phobic) weight percentage, block ratio, and side

Scheme 1. (a) Synthesis of norbornenyl-functionalized NHS ester 1, NB-NHS, (b) polymerization of glucose carbonates to afford NB-PGC<sub>a</sub>, 2, and (c) one-pot sequential ROMP of 1 and 2, followed by hydrolysis, to afford amphiphilic coil—brush block polymers 4,  $P(NB-COOH)_m$ -b- $P(NB-g-PGC_a)_n$ .

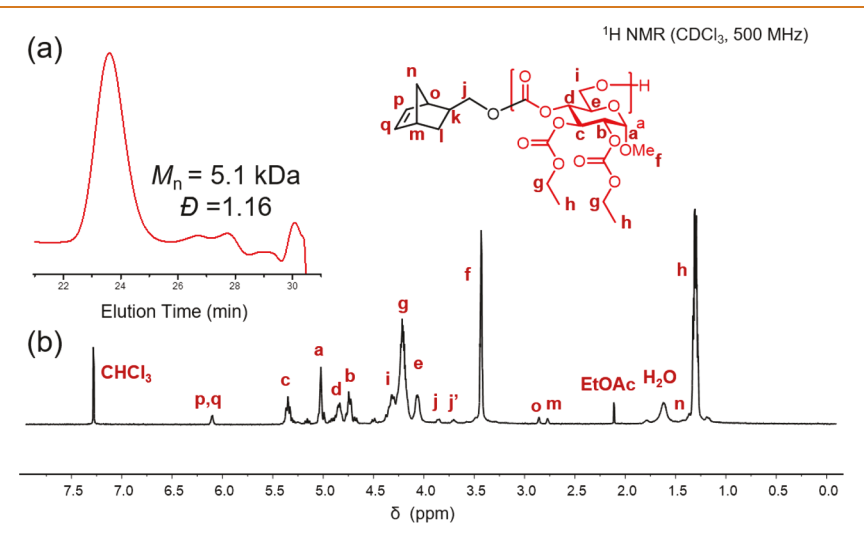


Figure 1. (a) SEC trace (THF as eluent, 1 mL/min) and (b)  $^{1}$ H NMR (500 MHz, CDCl<sub>3</sub>) spectrum of norbornene-terminated macromonomer 2b, NB-PGC<sub>17</sub>.

chain length, were investigated to study their individual and combined effects on the self-assembly behavior of coil—brush block polymers in aqueous media.

Synthesis of P(NB-COOH)-b-P(NB-g-PGC) Coil—Brush Block Polymers. As shown in Scheme 1, the synthesis of amphiphilic PGC-based coil-brush block polymers was achieved in four consecutive steps. First, norbornenylfunctionalized NHS ester 1 (NB-NHS) was synthesized in 83% yield by carbodiimide-mediated coupling of exonorbornene carboxylic acid and NHS in dichloromethane at room temperature followed by purification by flash chromatography. The structure was confirmed by electrospray ionization mass spectrometry (ESI-MS) and Fourier-transform infrared and <sup>1</sup>H and <sup>13</sup>C NMR spectroscopies (Figure S1). Second, a series of hydrophobic norbornene-terminated macromonomers 2 (Table S1) with different chain lengths was synthesized by organocatalyzed ROP of the bicyclic Dglucose-based carbonate monomer methyl-2,3-O-ethyloxycarbonyl-4,6-O-carbonyl-α-D-glucopyranoside at -78 °C using exo-5-norbornene-2-methanol as the initiator, according to a previously established procedure. 11 The resulting macromonomers were shown to have monomodal molar mass

dispersities ( $\theta < 1.1$ ) according to size exclusion chromatography (SEC) (Figure S2a). The molar masses were additionally determined by end group analysis from <sup>1</sup>H NMR spectroscopy (Figure 1) and by matrix-assisted laser desorption/ionizationtime-of-flight (MALDI-TOF) mass spectrometry (Figure S3). MALDI-TOF further confirmed the fidelity of the ROP and the presence of the norbornenyl-containing  $\alpha$ -chain end. Thermal properties were evaluated by thermogravimetric analysis (TGA) and differential scanning calorimetry (DSC) (Figures S4, S5). Third, sequential one-pot ROMP was performed at room temperature via the rapid addition of Grubbs' generation 3 (G3) catalyst as a solution in dichloromethane into a stock solution of coil-block precursor 1, followed ca. 15 min later by the quick addition of a relatively more concentrated solution of brush-block precursor macromonomer 2. The polymerizations were quenched by addition of ethyl vinyl ether 30 min after the macromonomer addition had occurred. These efficient polymerizations provided facile access to various coil-brush block polymers with low dispersities (D < 1.2) (Figure S2b-d), containing a linear NHS ester-functionalized block connected to a hydrophobic bottlebrush. The lengths of the two blocks were controlled by

Table 1. Characterization Data of P(NB-COOH)<sub>m</sub>-b-P(NB-g-PGC<sub>a</sub>)<sub>n</sub> Coil-Brush Polymers 4

	coil-brush block polymer	A/G <sup>a</sup>	$M_{\text{n NMR}}^{b}$ (kDa)	$M_{\text{n SEC}}^{b,c}$ (kDa)	$\mathcal{D}^{c}$	hydrophilic weight percentage (%)
A	$P(NB-COOH)_{54}-b-P(NB-g-PGC_{33})_5^d$	0.33	73.4	69.4	1.06	11
В	$P(NB-COOH)_{89}$ - $b$ - $P(NB-g$ - $PGC_{33})_5$	0.54	81.6	106	1.02	17
C	$P(NB-COOH)_{26}$ - $b$ - $P(NB-g$ - $PGC_{25})_5$	0.21	52.2	38.9	1.06	7
D	$P(NB-COOH)_{59}$ - $b$ - $P(NB-g$ - $PGC_{25})_5$	0.47	60.0	58.9	1.05	15
E	$P(NB-COOH)_{29}$ - $b$ - $P(NB-g$ - $PGC_{17})_3$	0.56	25.8	15.8	1.06	17
F	$P(NB-COOH)_{114}$ - $b$ - $P(NB-g$ - $PGC_{17})_7$	0.96	71.0	52.6	1.02	26
G	$P(NB-COOH)_{322}$ - $b$ - $P(NB-g$ - $PGC_{20})_{12}$	1.34	165.0	139	1.09	33
Н	$P(NB-COOH)_{173}$ - $b$ - $P(NB-g$ - $PGC_{25})_5$	1.38	86.8	107	1.02	34
I	$P(NB-COOH)_{143}$ - $b$ - $P(NB$ - $g$ - $PGC_{33})_2$	2.16	57.9	55.1	1.09	45
J	$P(NB-COOH)_{159}$ - $b$ - $P(NB-g$ - $PGC_{18})_7$	1.26	84.1	98.0	1.07	32
K	$P(NB-COOH)_{139}$ - $b$ - $P(NB-g$ - $PGC_{17})_4$	2.04	57.9	37.8	1.03	43
L	$P(NB-COOH)_{157}$ - $b$ - $P(NB-g$ - $PGC_8)_{12}$	1.64	73.3	103	1.04	37

"Molar ratio of carboxylic acid units to glucose carbonate units, calculated by comparing the peak integrals of NHS proton resonances with methyl group proton resonances from glucose carbonate repeating units, based on <sup>1</sup>H NMR spectra. <sup>b</sup>Molar masses here refer to the molar masses of the coil—brush block polymers having NHS groups. <sup>c</sup>Measured by THF SEC equipped with a multiangle laser light scattering (MALLS) detector. <sup>d</sup>DP<sub>n</sub>s were calculated by comparing the peak integrals from the corresponding characteristic proton resonances from each block.

adjusting the feed ratio between the (macro)monomers and Grubbs' G3 catalyst. Finally, to produce hydrophilic coil segments and enable supramolecular assembly in water, the NHS groups were cleaved by hydrolysis in a mixture of water and dimethylformamide (DMF) containing N,N-diisopropylethylamine (DIPEA), which was allowed to stir overnight at room temperature. The reaction mixtures were then transferred to dialysis tubings and dialyzed against nanopure water for at least 3 days, followed by being lyophilized to afford the final amphiphilic coil-brush polymers A-L. <sup>1</sup>H NMR and FT-IR spectroscopies confirmed the complete consumption of the NHS esters by showing that the proton NMR resonance at 2.82 ppm disappeared and a broad O-H stretch appeared from 3745 to 2756 cm<sup>-1</sup> (Figure S6). Taken together, these results demonstrate the successful synthesis of coil-brush block polymers composed of a coil block of hydrophilic norbornene carboxylic acid units and a bottlebrush block of hydrophobic poly(glucose carbonate)-grafted polynorbornene (Table 1). Notably, the NHS-functionalized precursor is anticipated to enable diversification of these coil-brush block polymers with a variety of amine-terminated moieties. The combination of ROP, "grafting-through" ROMP, and postpolymerization modification strategies for the hydrophobic and hydrophilic segments provided significant structural control and simultaneous incorporation of multiple functional moieties.

Although the architecture of the coil—brush block polymer is complex, the hydrophilic—hydrophobic balance was hypothesized to be the main factor governing the assembly behavior. We introduced the parameter A/G, *i.e.*, molar ratio of carboxylic acid units to glucose carbonate units,  $\frac{m}{a \times n}$ , to express the hydrophilic/hydrophobic content of the coil—brush block polymers, for evaluation of the self-assembly. The A/G ratio is calculated by comparing the integrals of the proton resonances of the methylene groups of the NHS esters  $(\delta = 2.82 \text{ ppm})$  with those of the methyl groups of the glucose carbonates  $(\delta = 1.29 \text{ ppm})$  (Figure 2).

Aqueous Solution Assembly of P(NB-COOH)-b-P(NB-g-PGC) Asymmetric Amphiphilic Coil—Brush Block Polymers. Aqueous assembly of the well-defined coil—brush block polymers at various A/G ratios and PGC side chain lengths was investigated using a dialysis-based solvent exchange process. In a typical experiment, coil—brush block

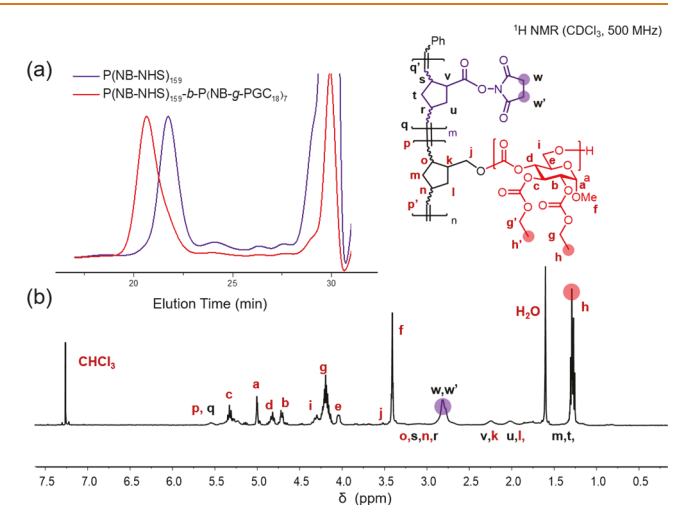


Figure 2. (a) Normalized SEC traces (THF as eluent, 1 mL/min) and (b)  $^1\text{H}$  NMR (500 MHz, CDCl<sub>3</sub>) spectrum of the sequential ROMP for preparation of coil-brush block polymer P(NB-NHS) $_{159}$ -b-P(NB-g-PGC $_{18}$ ) $_7$ .

polymers were dissolved in DMF at 1 mg/mL at room temperature, followed by extensive dialysis against nanopure water for 3 days. A strong Tyndall light scattering path was observed, suggesting the existence of assemblies. The size and morphology of the resulting nanostructures were characterized quantitatively by dynamic light scattering (DLS) and transmission electron microscopy (TEM). Assembly results were observed for all coil—brush block polymers, where a clear morphological transition between spherical micelles, long cylindrical nanostructures, and bilayer vesicles can be visualized by changing block polymer composition, *i.e.*, polymeric side chain lengths and overall hydrophilic/hydrophobic ratio.

Adjusting the Morphology by Changing the A/G Ratio and Brush Side Chain Length. As shown in the TEM images, vesicular structures with an average diameter of  $125 \pm 14$  nm and membrane thickness of  $15 \pm 5$  nm (Figure 3b,c) were observed from coil-brush block polymer A, P(NB-COOH)<sub>54</sub>-b-P(NB-g-PGC<sub>33</sub>)<sub>5</sub>, with a relatively low A/G ratio, 0.33, and long PGC side chains with a degree of polymerization  $(DP_n)$  of 33. The vesicular morphology was further

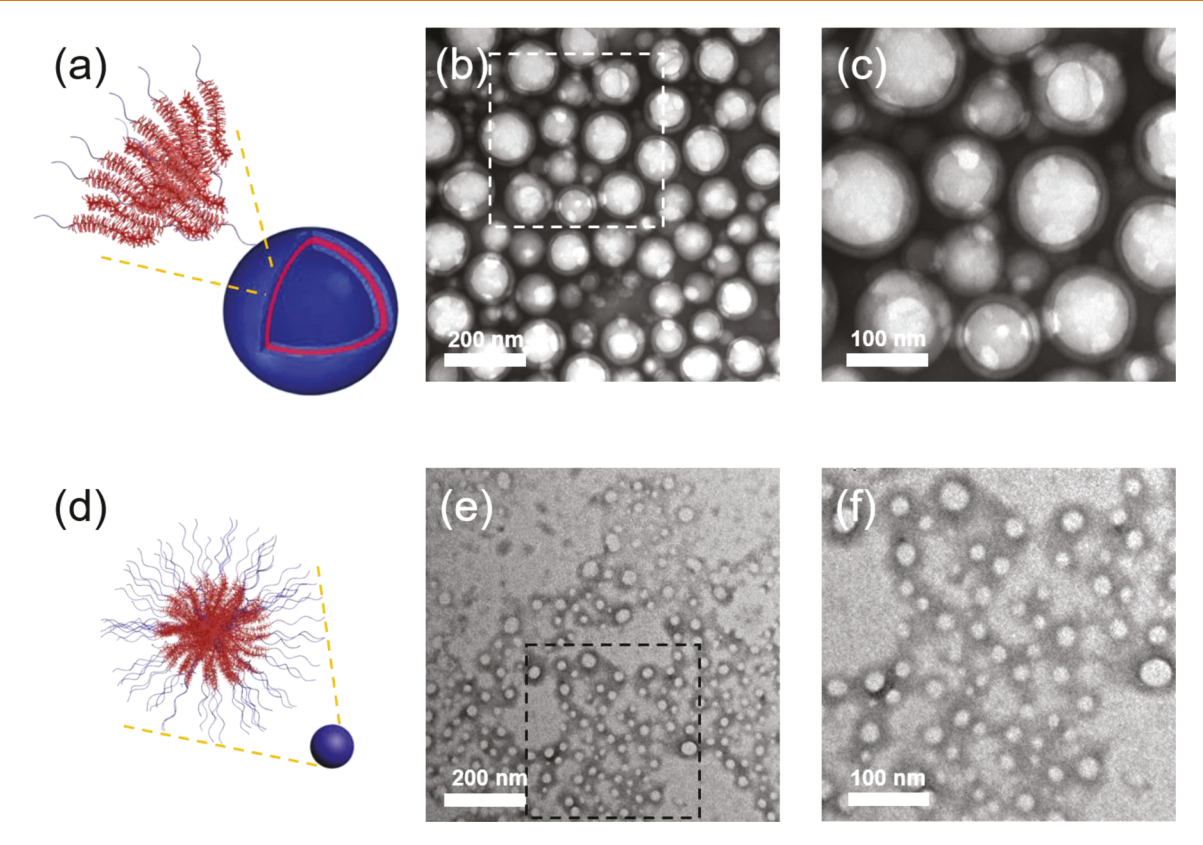


Figure 3. TEM analysis of assemblies obtained from coil—brush block polymers A (b, c) and I (e, f). TEM samples were negatively stained with 1 wt % phosphotungstic acid aqueous solution (20  $\mu$ L), and diameters were measured by counting >50 nanoparticles. Schematic illustrations of vesicles (a) and spherical micelles (d) composed of coil—brushes.

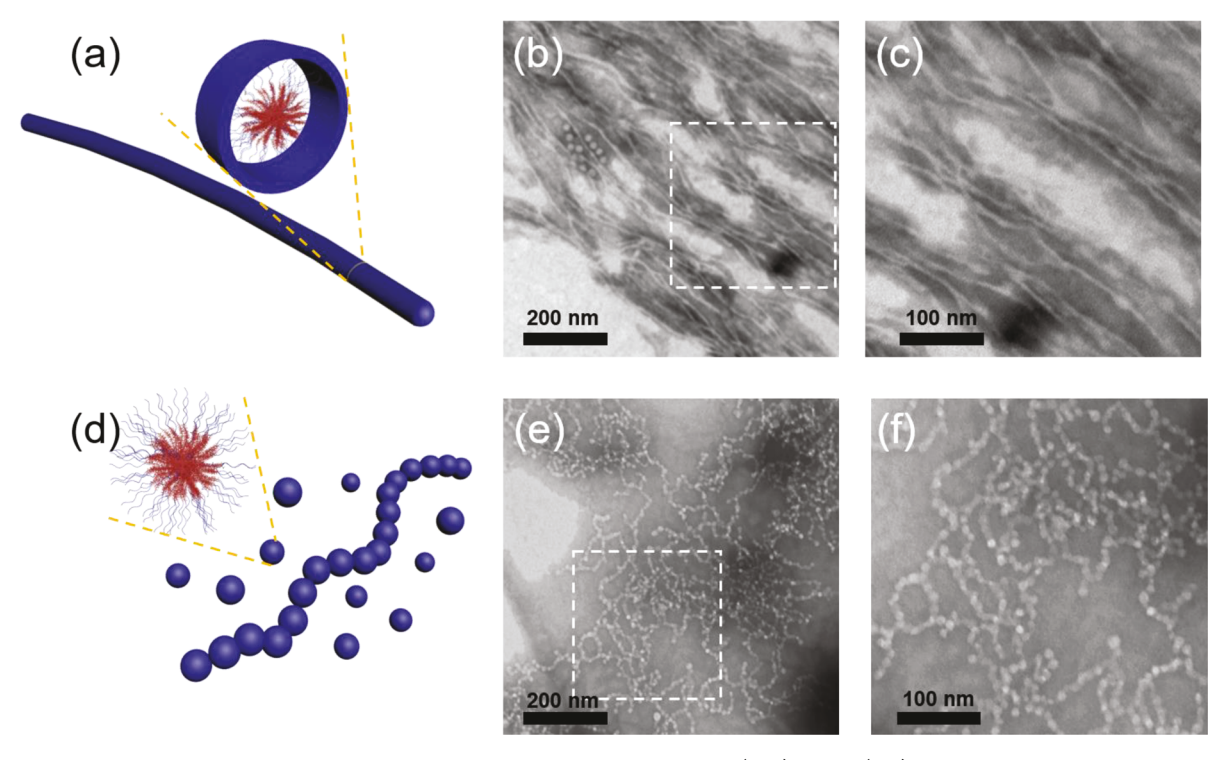


Figure 4. TEM analysis of assemblies obtained from coil—brush block polymers E (b, c) and F (e, f). TEM samples were negatively stained by 1 wt % phosphotungstic acid aqueous solution (20  $\mu$ L). Schematic illustrations of elongated cylindrical nanostructures (a) and pearl-necklace-like nanostructures (d) composed of coil—brushes.

supported by atomic force microscopy (AFM), illustrating apparent collapse on the substrate and cryo-TEM imaging with

observation of a double-layered structure (Figure S9). Maintaining the same side chain length, spherical micelles

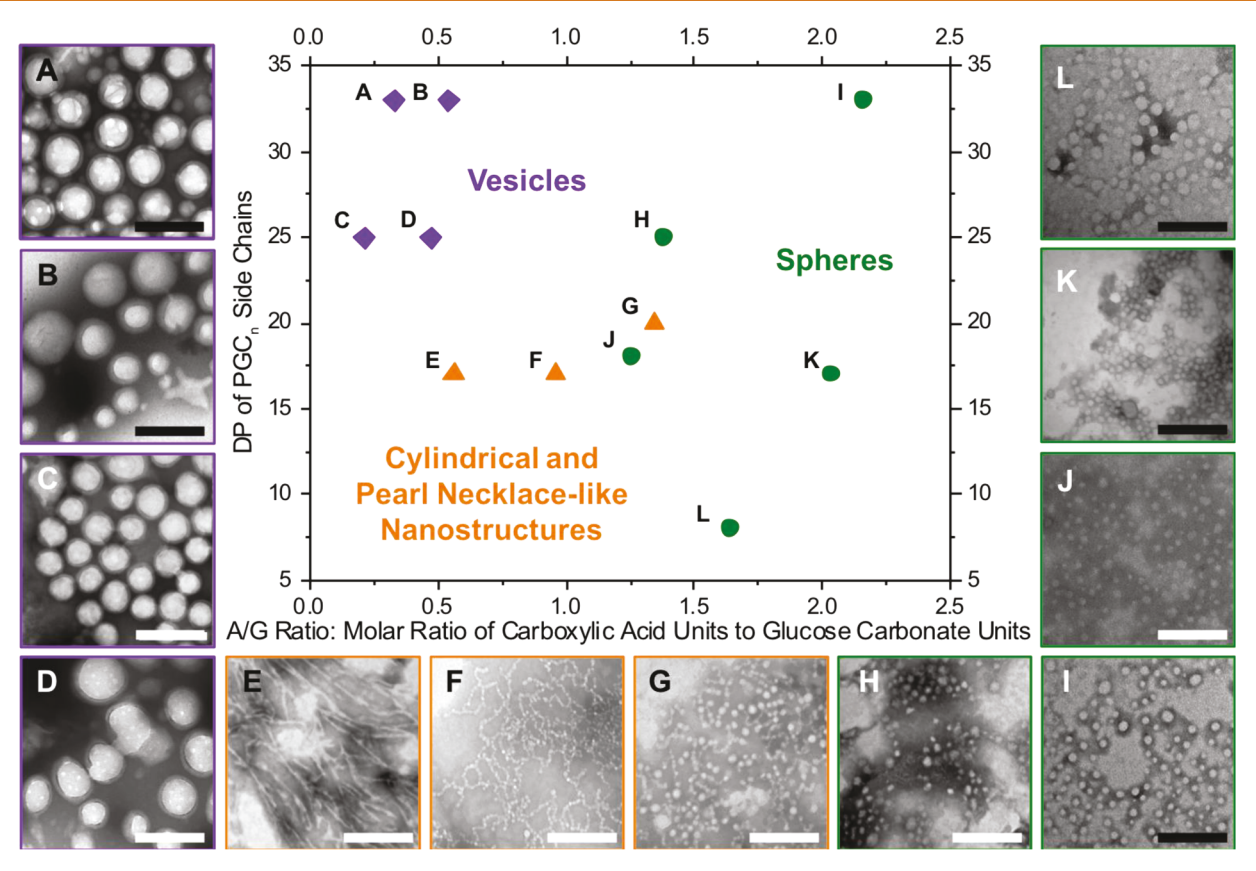


Figure 5. Phase diagram constructed for coil-brush block polymers A-L. As the side chain length and hydrophobic-hydrophilic ratio were systematically varied, the resulting morphologies included long cylinders (orange), vesicles (purple), and spheres (green). TEM samples were negatively stained by 1 wt % phosphotungstic acid aqueous solution (20  $\mu$ L). Scale bars represent 200 nm.

with an average diameter of  $28 \pm 5$  nm as measured by TEM (Figure 3e,f) and height of ca.  $3.5 \pm 1.0$  nm as measured by AFM (Figure S10) were obtained from coil-brush block polymer I,  $P(NB-COOH)_{143}$ -b-P(NB-g- $PGC_{33})_2$ , upon increasing the hydrophilic weight percentage to A/G = 2.16. The larger diameter relative to the height is expected to result from deformation of the particles upon adsorption onto the solid substrates for analyses. DLS showed unimodal size distributions of the vesicles and spheres, with number-average hydrodynamic diameters  $(D_{h(number)})$  of 150  $\pm$  50 nm and 60  $\pm$ 20 nm, respectively (Figure S11). The difference between absolute particle diameter values between DLS and TEM data could be attributed to the differences between their hydrated structure in the solvated state as measured by DLS and their structure in the dry state upon deposition onto a solid carboncoated copper grid substrate as measured by TEM, especially when these nanoassemblies are formed by coil-brush block polymers with flexible hydrophilic segments and stiff hydrophobic segments. The morphological variation between vesicular assemblies and spherical micelles may be due to a larger volume fraction of hydrophilic coil blocks, or coronal chains, of coil-brush I in aqueous solution, relative to A.

Vesicular structures were also dominant in coil—brush **B**,  $P(NB-COOH)_{89}$ - $b-P(NB-g-PGC_{33})_5$ , mainly due to the relatively long brush side chains and a similar A/G ratio compared to **A**. With similar A/G ratios of coil—brush block polymers **B** and **E**,  $P(NB-COOH)_{29}$ - $b-P(NB-g-PGC_{17})_3$ , *i.e.*, A/G ratios = 0.54 and 0.56, respectively, the lengths of their hydrophobic brush side chains varied markedly. As the  $DP_n$  of the grafted hydrophobic side chains decreased from 33 (**B**) to

17 (E), long cylindrical nanostructures with a width of 8  $\pm$  1 nm were observed by TEM (Figure 4b,c, Figure S12) and AFM (Figure S13). It is inferred that these long cylindrical micelles result from an arrangement where polymer chains adopted more curved interfaces between coil segments and brush segments than vesicular structures, which would be caused by shorter hydrophobic brush side chains, or a smaller core volume fraction in aqueous solution. Additionally, pearlnecklace-like nanostructures were found by TEM (Figure 4e,f) and AFM (Figure S14) for coil-brush F, P(NB-COOH)<sub>114</sub>-b- $P(NB-g-PGC_{17})_7$ , having the same polymeric side chain length and slightly higher A/G ratio than coil-brush E; thus, the pearl-necklace-like nanostructures can be considered as an intermediate between spherical and long cylindrical micelles, which warrants further investigation on the self-assembly mechanisms. For instance, TEM imaging of F after 3 days showed both pearl necklace and cylindrical nanoassemblies and, qualitatively, the pearl-necklace-like nanostructures were observed to evolve to a cylindrical morphology over longer time periods (Figure S15). The three-dimensional structural information for their higher-order supramolecular assembly was confirmed by tomographic TEM studies, as illustrated in a series of still and video images (Figure S16). When the coil segment was extended further, for example, A/G ratio increasing to 2.04 for coil-brush K, P(NB-COOH)<sub>139</sub>-b-P(NB-g-PGC<sub>17</sub>)<sub>4</sub>, TEM revealed spherical nanostructures.

On the basis of the above assembly of a library of coil—brush polymers with a range of side chain polymer lengths and A/G ratios, we proposed a roughly sectionalized phase diagram (Figure 5). Variation of the side chain length and hydrophilic—

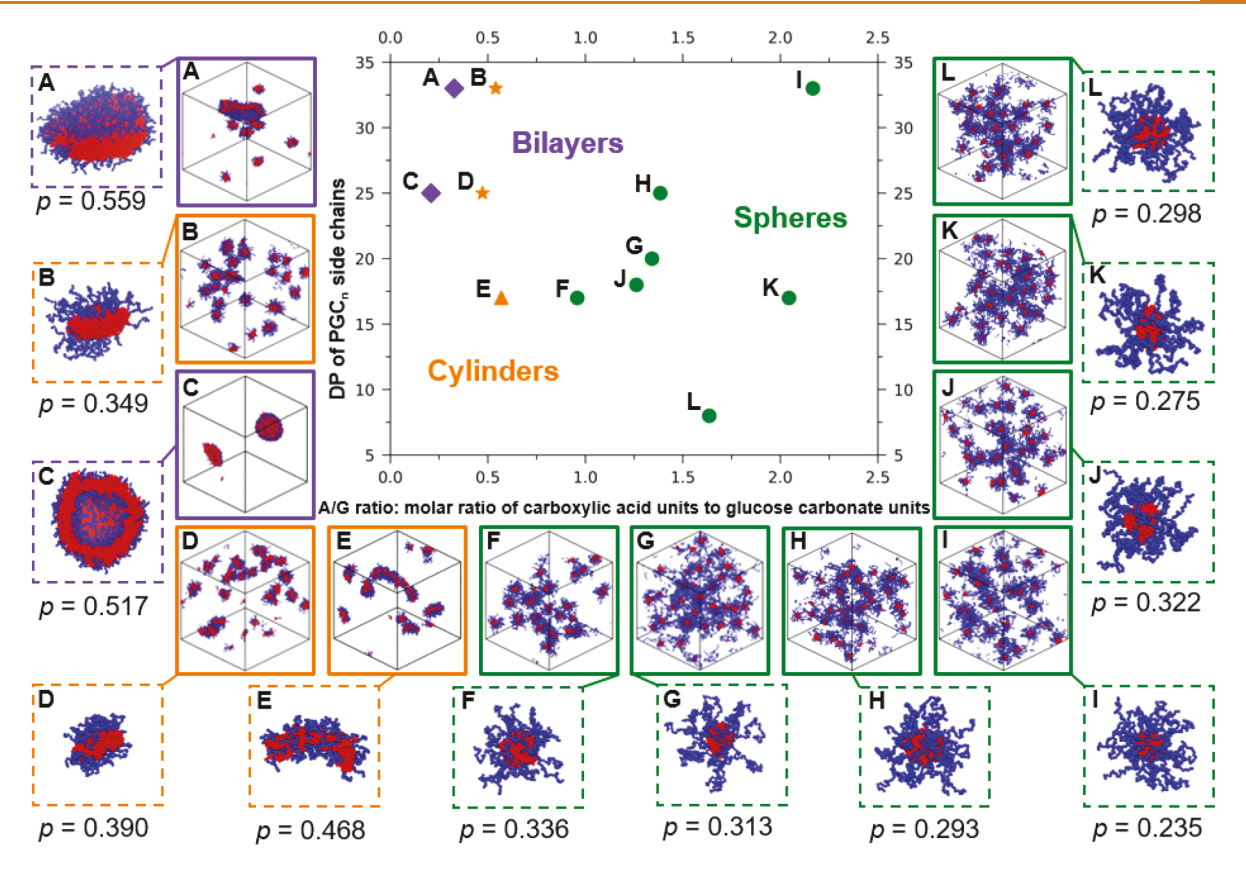


Figure 6. Phase diagram of assembled states from CG simulations of coil—brush polymers (A–L) conducted at 1 mg/mL polymer concentration. The assembled states including cylinders (orange triangles), disc-like structures (orange stars), bilayers (purple diamonds), and spheres (green spheres) are shown as a function of the side chain length and hydrophobic—hydrophilic ratio. In addition to representative assembled states (boxes with solid borders) one representative assembled micelle for each state is also shown (boxes with dashed borders) at different scales for visual clarity. The calculated packing parameter (p) for each assembled micelle is also indicated below the relevant micelle shape.

hydrophobic ratio dictated the morphology of the nano-objects formed by asymmetric coil—brushes upon aqueous assembly.

Simulations Using a Coarse-Grained Model of the Coil-Brush Block Polymers. To complement the experiments and provide understanding of the molecular packing within the assemblies, we conducted simulations using an intermediate-resolution coarse-grained (CG) model of the coil-brush block polymers; the details of this CG model are described in the Methods section (see Figure S7). In Figure 6, we present the phase diagram and representative snapshots of the assembled states seen in simulations as the side chain length and the A/G ratio (ratio of solvophilic/solvophobic degree of polymerization) were varied.

There is qualitative agreement between experiments (Figure 5) and simulations (Figure 6) in how the assembled state and the core—corona interfacial curvature changed with side chain length and A/G ratio. The spherical micelles, which have the highest curvature of all the morphologies, were observed in both simulations and experiments for the assembled states of coil—brush block polymers H, I, J, K, and L with high A/G ratios. At fixed side chain length, decreasing the A/G ratio (e.g., 1.26 J to 0.56 E) decreased the interfacial curvature and the morphologies transition from spherical shapes (in both experiments and simulations) to cylindrical shapes. At approximately the same A/G ratio, increasing the side chain length (e.g.,  $DP_n = 17$  in E to 33 in A) decreased the interfacial curvature, as the morphology transitioned from cylindrical nanostructures to vesicles (in experiments)/bilayers (in

simulation). The bilayers and cylinders in the simulations are analogous to the larger scale vesicles and longer cylindrical micelles in experiments, respectively. The chains in the vesicles are expected to arrange in a bilayer manner, and similarly elongated cylindrical nanostructures are the larger scale version of cylinders (see Figure S20).

To connect the changing interfacial curvature with known trends for polymer chain packing parameter, p, we calculated p of the chains in the assembled state (as described in Simulation Analyses). The p obtained for each of the assembly structures is shown in Figure 6 and agrees well with known trends of p and the observed micelle shapes<sup>71</sup> (see Figure S20). For example, in simulations at a fixed A/G ratio of ~0.3, we see that by decreasing the side chain length the morphology transitioned from bilayers (see micelle snapshot in  $\mathbf{A}$  with  $DP_{\rm n} = 33$ ) to vesicles (see micelle snapshot in  $\mathbf{C}$  with  $DP_{\rm n} = 25$ ) in Figure 5. The corresponding change in p follows the expected trend of Israelachvili and co-workers.

There are some *quantitative* differences between the experimental and computational phase diagrams (Figures 5 and 6). In experiments, at an A/G ratio of  $\sim$ 0.5 with increasing side chain length, the morphology changed from cylindrical micelles to vesicles ( $DP_n = 17$  E to 33 B in Figure 5). In simulations, for the same variation, the morphology changed from cylindrical micelles to disc-like micelles ( $DP_n = 17$  E to 33 B in Figure 6). Thus, the qualitative trend of changing interfacial curvature with the A/G ratio and side chain length is the same in both simulation and experiments; however, the

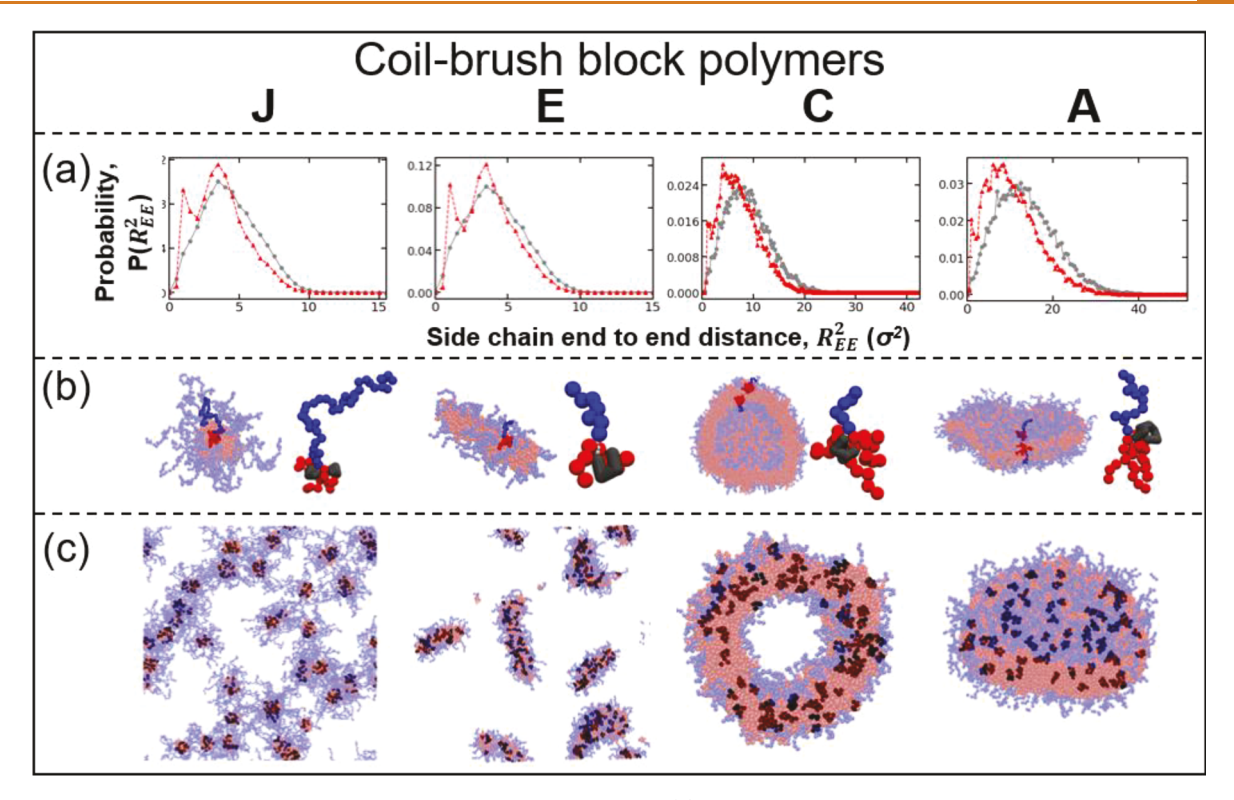


Figure 7. Side chain conformations for coil—brush polymers J, E, C, and A. (a) Probability distributions of the side chain squared end to end distances,  $P(R_{\rm EE}^2)$  versus  $R_{\rm EE}^2$ , at low solvophobicity (in disordered state, gray) and at high solvophobicity (upon assembly, red). (b) Representative assembled micelle structure and chain conformations; in black are side chains that loop back to the backbone with an  $R_{\rm EE}^2 < 2\sigma^2$ . (c) Representative snapshots of the assembled state with all side chains that adopt  $R_{\rm EE}^2 < 2\sigma^2$  shown in black. All images are at different scales for visual clarity.

phase boundaries in the phase diagrams do not match quantitatively between simulations and experiments. These phase boundaries can be adjusted through the CG model definition (Figures S7, S17), and we have selected the model that gives the best qualitative match in phase diagram with experiments, while maintaining reasonable computational speed, to further elucidate the chain packing and the conformations that the chains adopt within these micellar structures

Effect of Assembly on the Simulated Chain Conformations. In Figure 7a, the conformational changes in the side chains of the coil-brush block polymers J, E, C, and A upon micellization are shown through shifts in the distribution of the side chain squared end-to-end distances,  $R_{\rm EE}^2$ . The emergence of bimodal features in the distribution of  $R_{\text{EE}}^2$  upon assembly (at poorer solvent conditions/higher solvophobicity,  $\varepsilon_{\mathrm{BB}}$ , indicated in Figure S19) suggests a population of conformations with  $R_{\rm EE}^2 < 2\sigma^2$  and another population at the higher  $R_{\rm EE}^2$ . Side chains with  $R_{\rm EE}^2 < 2\sigma^2$  loop back to the backbone in a collapsed conformation, visualized in black in Figure 7b. These collapsed chains were well dispersed throughout the system, occurring in most of the micelles (Figure 7c), regardless of the morphology. We conjecture that, in general, the coil-brush block polymers with brush hydrophobic cores yielded frustrated packing in the micelle cores, and this led to some of the side chains sacrificing their conformational entropy to reduce the packing frustration, leading to an increased volume (i.e., possibility to explore conformations, and thus higher conformational entropy) for the remaining side chains within the micelle cores.

The discussion accompanying Figure S19 provides additional details of chain conformation calculations/visualization.

Comparison between Experimental and Simulation Spherical Micelle Sizes. The core radius of the spherical micelles shows quantitative agreement between experiments (measured from TEM images) and simulation (measured using two different metrics: the radius of gyration and the concentration profile) in Figure S21, although we see that the total micelle sizes are larger in the simulation than in the experiments, which is expected to be due to complications with identification of the outer surface of the micelles by the TEM imaging using negative staining. The technique of measuring the center-to-center distances for particle pairs that appeared to be in contact may have generated artificially low radii values, originating from particle—particle interactions and compression of the shell during the drying process.

## **CONCLUSIONS**

With the rapidly growing interest in the manufacture of materials that are translated from fundamental development to practical implementation to address societal needs, there is an increasing opportunity to harness the powerful advances that can come from integrating experimental techniques with computational tools. In this work, a series of well-defined P(NB-COOH)-b-P(NB-g-PGC) coil—brush block polymers that possess interesting features, including broad compositional, structural, and morphological design space, were prepared through a combination of ROP and ROMP, and their self-assembly behaviors in aqueous solutions were explored by experiments and simulations. We probed the impact of altering the side chain length and overall hydro-

philic-hydrophobic ratio on the nanoscopic morphology. In general, the less hydrophilic coil-brush block polymers tended to form vesicles or cylinders, while the more hydrophilic polymers yielded spherical structures and pearl-necklace-like nanostructures; pearl-necklace-like nanostructures were observed at intermediate hydrophilic-hydrophobic compositions. The length of the hydrophobic side chains was found to determine the interfacial curvature between the hydrophilic corona and hydrophobic core and, thereby, impact morphology. The qualitative agreement between experiments and simulations validates the coarse-grained model and enables the predictive design of nanostructures from this glucose-based coil-brush polymer platform while providing a fundamental understanding of interactions within solution assembly of complex polymer building blocks. Our findings expand the library of brush polymer assemblies and probe the architecture-morphology relationships of these glucose-based coil-brush block polymers through experimental and simulation tools.

Moreover, the degradable sugar-based coil-brush component and facile assembly in aqueous environment make these coil-brush block polymers promising nanomaterials for biological and environmental impact. For instance, toward biomedical applications, diverse morphologies are known to impart various benefits: conventional spherical micelles are able to load hydrophobic cargos, whereas vesicles have the potential to carry both hydrophobic and hydrophilic cargos at the same time and have even been employed as nanoreactors by accommodating hydrophobic cargo in the membrane and hydrophilic cargo in the interior.<sup>3,74</sup> Cylindrical nanostructures are of great interest owing to their large contact area with target tissues, longer in vivo circulation times, preference for altered cell-internalization pathways compared to spheres, With respect to the architecture of coil-brush building blocks, hydrophilic coronas consisting of linearshaped segments are known to provide highly tunable pathways for cargo release, for instance, cross-linking or grafting additional side chains to hinder release of encapsulated compounds.<sup>78</sup> Additionally, PGC-based cores with the potential to break down into natural byproducts are anticipated to enable controlled cargo release upon degradation. With respect to limiting the long-term environmental impact of polymer materials, increasing attention is being directed toward the construction of functional polymers from natural building blocks and also to building in mechanisms for degradation or recycling. 79,73,80-84 These poly(glucose carbonate)s offer advantages in both directions. Further studies involve the utilization of these combined experiments and simulations to produce increasingly complex nanostructures, derived from natural building blocks to afford functional properties and allow for mechanisms for their subsequent breakdown.

# **METHODS**

Materials. The bicyclic glucose-based carbonate monomer methyl-2,3-O-ethyloxycarbonyl-4,6-O-carbonyl-α-D-glucopyranoside (GC)<sup>11</sup> and the Grubbs G3 catalyst<sup>85</sup> were synthesized according to previously published procedures. 3-(3-Dimethylaminopropyl)-1-ethylcarbodiimide hydrochloride (EDC hydrochloride) was purchased from Chem-Impex International, Inc. 1,5,7-Triazabicyclo[4.4.0]dec-5-ene (TBD) was received from TCI America (Portland, OR, USA), degassed, and stored in a glovebox under an Ar atmosphere. Other chemicals and reagents were purchased from Sigma-Aldrich, Co. (St. Louis, MO, USA) and were used as received, unless otherwise noted.

Dichloromethane (DCM) and N,N-dimethylformamide (DMF) were dried using a solvent purification system (J. C. Meyer Solvent Systems, Inc., Laguna Beach, CA, USA). Nanopure water (18 M $\Omega$ cm) was obtained from a Milli-Q water filtration system (Millipore Corp, USA). Dialysis membrane tubing with a molar mass cutoff (MWCO) of 6–8 kDa was purchased from Spectrum Laboratories, Inc. (Rancho Dominguez, CA, USA) and soaked for 5 min in nanopure water at room temperature (rt) before use. Column chromatography was performed on a CombiFlash Rf4x (Teledyne ISCO) with RediSep Rf columns (Teledyne ISCO).

Instrumentation. <sup>1</sup>H NMR and <sup>13</sup>C NMR spectra were recorded on a Varian Inova 500 spectrometer (Varian, Inc., Palo Alto, CA, USA) interfaced to a UNIX computer using the VnmrJ software. Chemical shifts for <sup>1</sup>H NMR and <sup>13</sup>C NMR signals were referenced to the solvent resonance frequencies. Fourier transform infrared (FT-IR) spectra were recorded on an IR Prestige 21 system, equipped with a diamond attenuated total reflection (ATR) lens (Shimadzu Corp., Japan), and analyzed using IRsolution v. 1.40 software.

Size exclusion chromatography (SEC) was used to determine polymer molar mass and molar mass distribution (or dispersity, Đ). Polymer solutions were prepared at a known concentration (3-5 mg/ mL), and 200  $\mu$ L of an injection volume was used. After filtration through a 0.45  $\mu$ m PTFE filter, the polymer samples were passed through the SEC system equilibrated at 40 °C in tetrahydrofuran (THF) as the mobile phase with a flow rate of 1 mL/min. SEC was conducted on a Waters 1515HPLC (Waters Chromatography, Inc.) equipped with a differential refractive index (RI) detector (Wyatt Technology, Optilab T-rEX), a multiangle laser light scattering (MALLS) detector (Wyatt Technology, DAWN HELEOS II, 658 nm) using ASTRA software (Wyatt Technology; the dn/dc values of the analyzed polymers were determined from the differential refractometer response based on sample concentration, assuming 100% mass recovery), and a three-column series (Phenogel 5  $\mu$ m; 100 Å (Å), 104 Å, and linear (2);  $300 \times 4.6 \text{ mm}$  (mm) columns; Phenomenex, Inc.).

Glass transition temperatures  $(T_{\rm g})$  were measured by DSC on a Mettler-Toledo DSC3/700/1190 (Mettler-Toledo, Inc., Columbus, OH, USA) under a nitrogen gas atmosphere. Measurements were performed with a heating and cooling rate of 10 °C/min, and three heating and cooling cycles were conducted. Measurements were analyzed using Mettler-Toledo STARe v. 15.00a software. The  $T_{\rm g}$  was taken as the midpoint of the inflection tangent of the third heating scan.

TGA was performed under an Ar atmosphere using a Mettler-Toledo TGA2/1100/464, with a heating rate of 10  $^{\circ}$ C/min. Data were analyzed using Mettler-Toledo STARe v. 15.00a software.

ESI-MS was performed using an Applied Biosystems PE SCIEX QSTAR instrument. MALDI-TOF MS was performed on a Microflex LRF mass spectrometer (Bruker Corporation, Billerica, MA, USA) in positive linear mode. Ions were generated by a pulsed nitrogen laser (337 nm, 25 kV), and 100 laser pulses were used per spectrum. trans-2-[3-(4-tert-Butylphenyl)-2-methyl-2-propylidene]malonitrile (DCTB) and potassium trifluoroacetate (KTFA) were used as a matrix and cationization reagent, respectively. The sample and matrix were prepared at 1 and 26 mg/mL, respectively, in chloroform, and KTFA was prepared at 1 mg/mL in acetone. The sample solution was mixed with the matrix and KTFA at a volumetric ratio of 2:5:1, and 1  $\mu$ L of the mixture was deposited onto a stainless-steel sample holder and dried in air prior to the measurement.

TEM images were collected on a JEOL 1200EX operated at 100 kV, and micrographs were recorded using an SIA-15C CCD camera. Samples for TEM were prepared as follows: 20  $\mu$ L of polymer solution in nanopure water (0.3 mg/mL) was deposited onto a carbon-coated copper grid, and after 1 min, excess solution was quickly wicked away by a piece of filter paper. The samples were then negatively stained with a 1 wt % phosphotungstic acid (PTA) aqueous solution (20  $\mu$ L). After 30 s, excess staining solution was quickly wicked away by a piece of filter paper, and the samples were left to dry under ambient conditions prior to imaging.

AFM was performed using a Multimode 8 system (Bruker) using a ScanAsyst-Air silicon nitride probe (k=0.4 N/m,  $f_0=70$  kHz, Bruker). AFM images were assessed with Nanoscope Analysis (Bruker). For AFM sample preparation, the solution of nanoparticles in nanopure water ( $20~\mu L$ ) at 0.3 mg/mL was deposited on the mica surface, followed by spin coating. The mica surface was allowed to dry in vacuo.

Cryogenic-TEM (CryoTEM) images were performed on a FEI Talos operated at an accelerating voltage of 200 keV. For vitrified grid preparation, the FEI Vitrobot system, an automated plunge freezing device, was used. First, a droplet (3  $\mu$ L) of polymer solution was deposited onto a plasma-treated lacey carbon grid and then blotted two or three times, with each blot lasting around 1 s. After blotting, the sample was allowed to relax for 2 s to achieve uniform liquid thickness and then quickly plunged into a liquid ethane reservoir. The grids were then transferred to liquid nitrogen until further imaging. The temperature during imaging was maintained at  $-178~\rm ^{\circ}C$  to avoid any liquid crystallization. All images were taken with a FEI Falcon II camera with 1 s exposure time.

DLS measurements were conducted using a Zetasizer Nano ZS instrument (Malvern Panalytical Ltd., Malvern, UK) equipped with a laser diode operating at 633 nm. Scattered light was detected at 175° and analyzed using a log correlator for a 0.5 mL sample in a disposable cell (capacity = 0.9 mL). The photomultiplier aperture and attenuator were adjusted automatically. The particle size distribution and distribution averages were calculated using particle size distribution analysis routines in Zetasizer 7.13 software. Number of accumulations and measurement duration were adjusted automatically. All measurements were repeated three times. The average diameter of the particles is reported as the intensity-, volume-, and number-average particle diameter from three measurements.

Synthesis of the Hydrophilic Precursor Monomer Bicyclo[2.2.1]hept-5-ene-exo-2-carboxylic Acid N-Hydroxysuccinimide Ester. In a 25 mL Schlenk flask charged with a stir bar, the exo-5-norbornenecarboxylic acid (283 mg, 2.05 mmol, 1.0 equiv), N-hydroxysuccinimide (320 mg, 2.78 mmol, 1.4 equiv), and N-(3-dimethylaminopropyl)-N'-ethylcarbodiimide hydrochloride (EDCI·HCl) (470 mg, 3.03 mmol, 1.5 equiv) were allowed to stir in 10 mL of anhydrous DCM for 20 h under nitrogen flow at room temperature. The reaction mixture was concentrated under reduced pressure, and N-hydroxysuccinimidyl ester was purified by flash chromatography (100% DCM as eluent) to afford 1 as a white powder (482 mg, 1.70 mmol, 83% yield): <sup>1</sup>H NMR (500 MHz, CDCl<sub>3</sub>)  $\delta$  ppm 6.19 (dd, J = 6, 3 Hz, 1H), 6.13 (dd, J = 6, 3 Hz, 1H), 3.25 (s, 1H), 2.99 (s, 1H), 2.81 (d, J = 4 Hz, 5H), 2.49 (dd, J = 9, 4 Hz, 1H), 2.03 (dt, J = 12, 4 Hz, 1H), 1.59–1.47 (m, 2H), 1.43 (d, J =9 Hz, 1H);  $^{13}$ C NMR (126 MHz, CDCl<sub>3</sub>)  $\delta$  ppm 171.63, 169.37, 138.62, 138.53, 135.26, 47.10, 46.39, 41.76, 40.29, 30.95, 25.61; FT-IR (ATR, cm<sup>-1</sup>) 3071–2876, 1806, 1779, 1736, 1331, 1200, 1060, 947, 841, 710, 644; HRMS calculated [M + H]<sup>+</sup> for C<sub>12</sub>H<sub>13</sub>NO<sub>4</sub>H<sup>+</sup> 236.0923, found 236.0896.

General Procedure for Synthesis of Hydrophobic Macromonomers, exo-Norbornene-Terminated Poly(glucose carbonate)s (NB-PGCs). To a solution of the monomer GC (100 mg, 0.275 mmol) in anhydrous DCM (500  $\mu$ L) was added exo-Snorbornene-2-methanol (1.11  $\mu$ L, 0.009 60 mmol). The catalyst TBD (2 mol % with respect to monomer, 0.766 mg, 0.00550 mmol) was added with stirring at  $-78~^{\circ}$ C for 5 min. The reaction was removed from the acetone—dry ice bath, quenched with excess addition of acetic acid, and evaporated for analysis by GPC-MALLS without purification. The polymers were precipitated three times into ice-cold methanol and dried under vacuum.

NB-PGC<sub>8</sub>: <sup>1</sup>H NMR (500 MHz, CDCl<sub>3</sub>)  $\delta$  ppm 6.09 (t, J = 5 Hz), 5.41–5.25 (m), 5.06–4.97 (m), 4.95–4.87 (m), 4.84 (dd, J = 11, 9 Hz), 4.79–4.70 (m), 4.38–4.21 (m), 3.39 (s), 1.40–1.24 (m), 1.21–1.13 (m); <sup>13</sup>C NMR (126 MHz, CDCl<sub>3</sub>)  $\delta$  ppm 206.92, 154.20, 154.07, 153.76, 96.33, 77.27, 73.69, 73.45, 72.75, 66.71, 66.01, 64.70, 64.66, 64.54, 55.62, 55.43, 30.91, 14.09; FT-IR (ATR, cm<sup>-1</sup>) 3080–2793, 1750, 1458, 1371, 1234, 1011, 872, 779. 90% yield; DSC  $T_{\rm g}$  = 62 °C; TGA in Ar 272–384 °C, 89% mass loss.

NB-PGC<sub>17</sub>: <sup>1</sup>H NMR (500 MHz, CDCl<sub>3</sub>)  $\delta$  ppm 6.09 (t, J = 4 Hz), 5.42–5.24 (m), 5.07–4.95 (m), 4.94–4.86 (m), 4.85–4.78 (m), 4.71 (dt, J = 11, 3 Hz), 4.36–4.26 (m), 4.26–4.12 (m), 4.04 (qd, J = 9, 7, 4 Hz), 3.41 (s, J = 1 Hz), 1.34–1.23 (m); <sup>13</sup>C NMR (126 MHz, CDCl<sub>3</sub>)  $\delta$  ppm 206.90, 154.10, 154.06, 153.75, 96.33, 73.70, 73.43, 72.75, 66.01, 64.69, 64.66, 64.54, 55.62, 14.10; FT-IR (ATR, cm<sup>-1</sup>) 3078–2785, 1751, 1458, 1373, 1234, 1011, 872, 779. 93% yield; DSC  $T_g$  = 85 °C; TGA in Ar 245–401 °C, 93% mass loss.

NB-PGC<sub>18</sub>: <sup>1</sup>H NMR (500 MHz, CDCl<sub>3</sub>)  $\delta$  ppm 6.09 (t, J = 4 Hz), 5.39–5.25 (m), 5.08–4.95 (m), 4.95–4.85 (m), 4.83 (dd, J = 11, 9 Hz, 7H), 4.38–3.96 (m), 3.41 (s), 1.38–1.18 (m); <sup>13</sup>C NMR (126 MHz, CDCl<sub>3</sub>)  $\delta$  ppm 154.10, 154.07, 153.75, 96.33, 73.69, 73.43, 72.75, 66.71, 66.01, 64.69, 64.66, 64.58, 55.62, 14.09; FT-IR (ATR, cm<sup>-1</sup>) 3078–2800, 1751, 1458, 1371, 1234, 1011, 872, 779. 95% yield; DSC  $T_{\rm g}$  = 89 °C; TGA in Ar 240–387 °C, 88% mass loss. NB-PGC<sub>20</sub>: <sup>1</sup>H NMR (500 MHz, CDCl<sub>3</sub>)  $\delta$  ppm 6.09 (m), 5.40–

NB-PGC<sub>20</sub>. H NMR (500 MHz, CDCl<sub>3</sub>)  $\delta$  ppm 6.09 (m), 5.40–5.30 (m), 4.88–4.79 (m), 4.79–4.69 (m), 4.37–3.68 (m), 3.45–3.39 (m), 1.92–1.29 (m);  $^{13}$ C NMR (126 MHz, CDCl<sub>3</sub>)  $\delta$  ppm 206.92, 154.10, 154.07, 153.75, 153.76, 96.32, 73.68, 73.42, 72.74, 72.41, 66.71, 66.01, 64.70, 64.67, 64.58, 64.54, 55.62, 14.10; FT-IR (ATR, cm<sup>-1</sup>) 3078–2800, 1751, 1458, 1371, 1234, 1011, 872, 779. 95% yield; DSC  $T_g$  = 93 °C; TGA in Ar 264–393 °C, 93% mass loss. NB-PGC<sub>25</sub>: H NMR (500 MHz, CDCl<sub>3</sub>)  $\delta$  ppm 6.11 (t, J = 4 Hz),

NB-PGC<sub>25</sub>: <sup>1</sup>H NMR (500 MHz, CDCl<sub>3</sub>)  $\delta$  ppm 6.11 (t, J = 4 Hz), 5.40–5.30 (m), 5.03 (t, J = 4 Hz), 4.84 (t, J = 10 Hz), 4.75 (ddt, J = 14, 10, 4 Hz), 4.34 (d, J = 13 Hz), 4.25 (s), 4.29–4.13 (m), 4.10–4.02 (m), 3.49–3.37 (m), 3.43 (s), 1.39–1.25 (m); <sup>13</sup>C NMR (126 MHz, CDCl<sub>3</sub>)  $\delta$  ppm 206.92, 154.24, 154.10, 154.07, 153.80, 153.76, 96.32, 77.27, 77.01, 76.76, 73.68, 73.42, 72.74, 72.41, 66.71, 66.00, 64.70, 64.67, 64.58, 64.54, 55.60, 55.43, 30.91, 14.10; FT-IR (ATR, cm<sup>-1</sup>) 3063–2801, 1751, 1458, 1373, 1234, 1018, 872, 779. 90% yield; DSC  $T_{\rm g}$  = 106 °C; TGA in Ar 195–390 °C, 91% mass loss. NB-PGC<sub>33</sub>: <sup>1</sup>H NMR (500 MHz, CDCl<sub>3</sub>)  $\delta$  ppm 6.09 (m), 5.34

NB-PGC<sub>33</sub>: <sup>1</sup>H NMR (500 MHz, CDCl<sub>3</sub>)  $\delta$  ppm 6.09 (m), 5.34 (dq, J = 11, 7, 6 Hz), 5.01 (dt, J = 8, 4 Hz), 4.83 (td, J = 10, 5 Hz), 4.75–4.65 (m), 4.32 (d, J = 13 Hz), 4.27–4.12 (m), 4.07–4.02 (m), 3.42 (d, J = 6 Hz), 1.29 (m); <sup>13</sup>C NMR (126 MHz, CDCl<sub>3</sub>)  $\delta$  ppm 206.90, 154.20, 154.07, 153.76, 96.33, 73.69, 73.43, 72.74, 66.01, 64.70, 64.66, 64.58, 55.62, 14.09; FT-IR (ATR, cm<sup>-1</sup>) 3071–2762, 1751, 1458, 1373, 1234, 1173, 1018, 872, 779. 90% yield; DSC  $T_{\rm g}$  = 110 °C; TGA in Ar 261–380 °C, 81% mass loss.

General Procedure for Sequential ROMP of NB-NHS Ester and NB-PGC. In a glovebox, 250  $\mu$ L of anhydrous DCM was added into vials containing NB-NHS monomer (5.0 mg, 21  $\mu$ mol) to form a solution with a monomer concentration of 0.02 g/mL. To a solution of Grubbs' G3 catalyst in DCM (3.14 mg/mL, 100  $\mu$ L) under argon in a glass vial capped with a septum was added a solution of NB-NHS monomer. The reaction was allowed to stir at rt for 15 min, and an aliquot of the reaction mixture (100  $\mu$ L) was withdrawn for the analysis of the first block. The solution of NB-PGC macromonomer (50.0 mg/mL) in 300  $\mu$ L of anhydrous DCM was then quickly added to the polymerization mixture and stirred for 30 min before addition of an excess amount of ethyl vinyl ether. The final coil—brush block polymers were obtained after precipitating the reaction mixture in diethyl ether twice and dried under vacuum overnight to yield white powders.

P(NB-NHS)<sub>54</sub>-*b*-P(NB-*g*-PGC<sub>33</sub>)<sub>5</sub>: <sup>1</sup>H NMR (500 MHz, CDCl<sub>3</sub>)  $\delta$  ppm 5.34 (t, J = 9 Hz, CH=CHs from brush backbone), 5.01 (d, J = 4 Hz, CHOCH<sub>3</sub> in NB-PGC units), 4.84 (t, J = 9 Hz, CHOCO in NB-PGC units), 4.72 (m, OCH<sub>2</sub>CH<sub>3</sub> in NB-PGC units), 4.19 (m, OCH<sub>2</sub>CH<sub>3</sub> in NB-PGC units), 3.42 (s, OCH<sub>3</sub> in NB-PGC units), 2.83 (m, CH<sub>2</sub>CH<sub>2</sub> from NHS units), 2.19 (d, J = 1.0 Hz, CH<sub>2</sub>s from PNB backbone), 1.29 (m, CH<sub>2</sub>CH<sub>3</sub> in NB-PGC units); <sup>13</sup>C NMR (126 MHz, CDCl<sub>3</sub>)  $\delta$  ppm 154.11, 153.76, 96.36, 77.26, 77.03, 76.72, 73.70, 73.45, 72.76, 66.71, 64.76, 64.58, 55.64, 14.10; FT-IR (ATR, cm<sup>-1</sup>) 3078–2762, 1751, 1458, 1373, 1234, 1010, 872, 779. 90% yield.

P(NB-NHS)<sub>89</sub>-b-P(NB-g-PGC<sub>33</sub>)<sub>5</sub>: <sup>1</sup>H NMR (500 MHz, CDCl<sub>3</sub>)  $\delta$  ppm 5.34 (t, J = 10 Hz, CH=CHs from brush backbone), 5.01 (d, J = 4 Hz, CHOCH<sub>3</sub> in NB-PGC units), 4.83 (t, J = 10 Hz, CHOCO in NB-PGC units), 4.72 (m, OCH<sub>2</sub>CH<sub>3</sub> in NB-PGC units), 4.27–4.11 (m, OCH<sub>2</sub>CH<sub>3</sub> in NB-PGC units), 3.45–3.39 (s, OCH<sub>3</sub> in NB-PGC

units), 2.82 (m, CH<sub>2</sub>CH<sub>2</sub> from NHS units), 1.35–1.25 (m, CH<sub>2</sub>CH<sub>3</sub> in NB-PGC units);  $^{13}$ C NMR (126 MHz, CDCl<sub>3</sub>)  $\delta$  ppm 154.11, 154.09, 153.75, 96.35, 77.35, 77.01, 76.75, 73.70, 73.45, 72.76, 66.71, 64.80, 64.68, 64.58, 55.64, 55.43, 14.12; FT-IR (ATR, cm<sup>-1</sup>) 2970, 1751, 1466, 1373, 1242, 1011, 872, 779. 87% yield.

P(NB-NHS)<sub>26</sub>-b-P(NB-g-PGC<sub>25</sub>)<sub>5</sub>: <sup>1</sup>H NMR (500 MHz, CDCl<sub>3</sub>)  $\delta$  ppm 5.35 (q, J = 9 Hz, CH=CHs from brush backbone), 5.03 (d, J = 4 Hz, CHOCH<sub>3</sub> in NB-PGC units), 4.85 (t, J = 10 Hz, CHOCO in NB-PGC units), 4.74 (d, J = 10 Hz, CHOCH<sub>3</sub> in NB-PGC units), 4.41–4.31 (m, OCH<sub>2</sub>CH<sub>3</sub> in NB-PGC units), 4.29–4.21 (m, OCH<sub>2</sub>CH<sub>3</sub> in NB-PGC units), 3.47–3.41 (s, OCH<sub>3</sub> in NB-PGC units), 2.82 (m, CH<sub>2</sub>CH<sub>2</sub> from NHS units), 1.40–1.22 (m, CH<sub>2</sub>CH<sub>3</sub> in NB-PGC units); <sup>13</sup>C NMR (126 MHz, CDCl<sub>3</sub>)  $\delta$  ppm 154.12, 153.78, 96.34, 77.35, 77.03, 76.71, 73.70, 73.43, 72.75, 66.72, 64.69, 64.60, 55.64, 30.94, 14.12; FT-IR (ATR, cm<sup>-1</sup>) 2978, 1750, 1452, 1374, 1242, 1011, 872, 778. 85% yield.

P(NB-NHS)<sub>59</sub>-*b*-P(NB-*g*-PGC<sub>25</sub>)<sub>5</sub>: <sup>1</sup>H NMR (500 MHz, CDCl<sub>3</sub>)  $\delta$  ppm 5.03 (d, J = 4 Hz, CHOCH<sub>3</sub> in NB-PGC units), 4.88–4.81 (m, CHOCO in NB-PGC units), 4.74 (d, J = 10 Hz, CHOCH<sub>3</sub> in NB-PGC units), 4.34 (m, OCH<sub>2</sub>CH<sub>3</sub> in NB-PGC units), 4.26–4.13 (m, OCH<sub>2</sub>CH<sub>3</sub> in NB-PGC units), 3.44 (s, OCH<sub>3</sub> in NB-PGC units), 2.82 (m, CH<sub>2</sub>CH<sub>2</sub> from NHS units), 1.40–1.23 (m, CH<sub>2</sub>CH<sub>3</sub> in NB-PGC units); <sup>13</sup>C NMR (126 MHz, CDCl<sub>3</sub>)  $\delta$  ppm 154.10, 154.09, 153.76, 96.36, 77.26, 77.04, 76.75, 73.69, 73.45, 72.76, 66.70, 64.76, 64.68, 64.58, 55.64, 55.43, 14.11; FT-IR (ATR, cm<sup>-1</sup>) 2980, 1751, 1450, 1373, 1234, 1011, 872, 780. 90% yield.

P(NB-NHS)<sub>29</sub>-b-P(NB-g-PGC<sub>17</sub>)<sub>3</sub>: <sup>1</sup>H NMR (500 MHz, CDCl<sub>3</sub>)  $\delta$  ppm 5.36 (m, CH=CHs from brush backbone), 5.03 (m, CHOCH<sub>3</sub> in NB-PGC units), 4.85 (m, CHOCO in NB-PGC units), 4.74 (d, J = 10 Hz, CHOCH<sub>3</sub> in NB-PGC units), 4.33 (m, OCH<sub>2</sub>CH<sub>3</sub> in NB-PGC units), 4.25–4.18 (m, OCH<sub>2</sub>CH<sub>3</sub> in NB-PGC units), 3.50 (s, OCH<sub>3</sub> in NB-PGC units), 2.82 (m, CH<sub>2</sub>CH<sub>2</sub> from NHS units), 1.36–1.26 (m, CH<sub>2</sub>CH<sub>3</sub> in NB-PGC units); <sup>13</sup>C NMR (126 MHz, CDCl<sub>3</sub>)  $\delta$  ppm 154.11, 154.10, 153.76, 96.35, 77.26, 77.00, 76.75, 73.69, 72.76, 66.70, 64.76, 64.69, 64.58, 55.64, 14.11; FT-IR (ATR, cm<sup>-1</sup>) 2980, 1750, 1451, 1373, 1242, 1010, 872, 779. 92% yield.

P(NB-NHS)<sub>114</sub>-*b*-P(NB-*g*-PGC<sub>17</sub>) $_7$ : <sup>1</sup>H NMR (500 MHz, CDCl<sub>3</sub>)  $\delta$  ppm 5.32 (br, CH=CHs from brush backbone), 5.02–4.95 (m, CHOCH<sub>3</sub> in NB-PGC units), 4.82–4.68 (m, CHOCO in NB-PGC units), 4.34–4.28 (m, OCH<sub>2</sub>CH in NB-PGC units), 4.22–4.15 (m, OCH<sub>2</sub>CH<sub>3</sub> in NB-PGC units), 4.09–4.02 (m, CHCH(CH<sub>2</sub>)O in NB-PGC units), 3.46–3.37 (s, OCH<sub>3</sub> in NB-PGC units), 2.82 (br, CH<sub>2</sub>CH<sub>2</sub> from NHS units), 2.25–2.02 (m, CH<sub>2</sub>s from PNB backbone), 1.35–1.23 (m, CH<sub>2</sub>CH<sub>3</sub> in NB-PGC units); <sup>13</sup>C NMR (126 MHz, CDCl<sub>3</sub>)  $\delta$  ppm 154.11, 154.09, 153.76, 96.36, 77.26, 77.01, 76.75, 73.69, 73.45, 72.76, 66.71, 64.76, 64.68, 64.58, 55.64, 55.43, 14.10; FT-IR (ATR, cm<sup>-1</sup>) 2978, 1751, 1450, 1380, 1242, 1011, 872, 779. 90% yield.

P(NB-NHS)<sub>322</sub>-b-P(NB-g-PGC<sub>20</sub>)<sub>12</sub>: <sup>1</sup>H NMR (500 MHz, CDCl<sub>3</sub>)  $\delta$  ppm 5.35–5.27 (m, CH=CHs from brush backbone), 5.00 (d, J = 4 Hz, CHOCH<sub>3</sub> in NB-PGC units), 4.81 (t, J = 10 Hz, CHOCO in NB-PGC units), 4.30 (d, J = 12 Hz, OCH<sub>2</sub>CH in NB-PGC units), 4.24–4.12 (m, OCH<sub>2</sub>CH<sub>3</sub> in NB-PGC units), 4.04 (m, CHCH(CH<sub>2</sub>) O in NB-PGC units), 3.43–3.38 (s, OCH<sub>3</sub> in NB-PGC units), 2.83–2.77 (m, CH<sub>2</sub>CH<sub>2</sub> from NHS units), 2.19–2.09 (m, CH<sub>2</sub>s from PNB backbone), 1.33–1.23 (m, CH<sub>2</sub>CH<sub>3</sub> in NB-PGC units); <sup>13</sup>C NMR (126 MHz, CDCl<sub>3</sub>)  $\delta$  ppm 154.10, 154.10, 153.76, 96.40, 77.26, 77.01, 76.75, 73.69, 73.45, 72.76, 66.70, 64.76, 64.68, 64.58, 55.64, 14.10; FT-IR (ATR, cm<sup>-1</sup>) 2982, 1751, 1450, 1373, 1234, 1011, 872, 780. 93% yield.

P(NB-NHS)<sub>173</sub>-*b*-P(NB-*g*-PGC<sub>25</sub>)<sub>5</sub>: <sup>1</sup>H NMR (500 MHz, CDCl<sub>3</sub>)  $\delta$  ppm 5.35 (t, J = 10 Hz, CH=CHs from brush backbone), 5.03 (m, CHOCH<sub>3</sub> in NB-PGC units), 4.84 (t, J = 10 Hz, CHOCO in NB-PGC units), 4.33 (d, J = 12 Hz, OCH<sub>2</sub>CH in NB-PGC units), 4.26–4.16 (m, OCH<sub>2</sub>CH<sub>3</sub> in NB-PGC units), 4.06 (m, CHCH(CH<sub>2</sub>)O in NB-PGC units), 3.43 (q, J = 2 Hz, OCH<sub>3</sub> in NB-PGC units), 2.82 (m, CH<sub>2</sub>CH<sub>2</sub> from NHS units), 2.27 (m, CH<sub>2</sub>s from PNB backbone), 1.34–1.18 (m, CH<sub>2</sub>CH<sub>3</sub> in NB-PGC units); <sup>13</sup>C NMR (126 MHz, CDCl<sub>3</sub>)  $\delta$  ppm 154.11, 154.09, 153.76, 96.36, 77.26, 77.03, 76.75, 73.69, 73.43, 72.76, 64.76, 64.68, 64.60, 55.64, 55.43, 14.10; FT-IR

(ATR,  $cm^{-1}$ ) 2950, 1750, 1450, 1373, 1234, 1011, 872, 779. 90% yield.

P(NB-NHS)<sub>143</sub>-*b*-P(NB-*g*-PGC<sub>33</sub>)<sub>2</sub>: <sup>1</sup>H NMR (500 MHz, CDCl<sub>3</sub>)  $\delta$  ppm 5.33 (d, J = 10 Hz, CH=CHs from brush backbone), 5.01 (d, J = 4 Hz, CHOCH<sub>3</sub> in NB-PGC units), 4.83 (dd, J = 12 Hz, CHOCO in NB-PGC units), 4.32 (d, J = 12 Hz, OCH<sub>2</sub>CH in NB-PGC units), 4.27–4.12 (m, OCH<sub>2</sub>CH<sub>3</sub> in NB-PGC units), 4.06 (dd, J = 11 Hz, m, CHCH(CH<sub>2</sub>)O in NB-PGC units), 3.49 (s, OCH<sub>3</sub> in NB-PGC units), 2.82 (s, CH<sub>2</sub>CH<sub>2</sub> from NHS units), 2.26 (m, CH<sub>2</sub>s from PNB backbone), 1.29–1.17 (m, CH<sub>2</sub>CH<sub>3</sub> in NB-PGC units); <sup>13</sup>C NMR (126 MHz, CDCl<sub>3</sub>)  $\delta$  ppm 154.10, 154.09, 153.76, 96.40, 77.26, 77.01, 76.75, 73.70, 73.45, 72.78, 66.71, 64.76, 64.68, 64.58, 55.65, 55.43, 14.11; FT-IR (ATR, cm<sup>-1</sup>) 2981, 1751, 1450, 1372, 1242, 1008, 872, 779. 91% yield.

P(NB-NHS)<sub>159</sub>-b-P(NB-g-PGC<sub>18</sub>)<sub>7</sub>: <sup>1</sup>H NMR (500 MHz, CDCl<sub>3</sub>) δ ppm 5.33 (d, J = 10 Hz, CH=CHs from brush backbone), 5.04–4.96 (m, CHOCH<sub>3</sub> in NB-PGC units), 4.84 (q, J = 11 Hz, CHOCO in NB-PGC units), 4.31 (m, OCH<sub>2</sub>CH in NB-PGC units), 4.27–4.12 (m, OCH<sub>2</sub>CH<sub>3</sub> in NB-PGC units), 4.08–4.02 (m, CHCH(CH<sub>2</sub>)O in NB-PGC units), 3.42 (s, OCH<sub>3</sub> in NB-PGC units), 2.82 (s, CH<sub>2</sub>CH<sub>2</sub> from NHS units), 2.26 (s, CH<sub>2</sub>s from PNB backbone), 1.29 (m, CH<sub>2</sub>CH<sub>3</sub> in NB-PGC units); <sup>13</sup>C NMR (126 MHz, CDCl<sub>3</sub>) δ ppm 154.10, 154.10, 153.76, 96.36, 77.30, 77.01, 76.76, 73.69, 73.45, 72.76, 66.72, 64.76, 64.68, 64.58, 55.65, 55.43, 14.11; FT-IR (ATR, cm<sup>-1</sup>) 2980, 1751, 1451, 1373, 1237, 1010, 872, 780. 90% yield.

P(NB-NHS)<sub>139</sub>-*b*-P(NB-*g*-PGC<sub>17</sub>)<sub>4</sub>: <sup>1</sup>H NMR (500 MHz, CDCl<sub>3</sub>)  $\delta$  ppm 5.57 (m, CH=CHs from brush backbone), 5.03 (d, J = 4 Hz, CHOCH<sub>3</sub> in NB-PGC units), 4.84 (t, J = 10 Hz, CHOCO in NB-PGC units), 4.27–4.13 (m, OCH<sub>2</sub>CH<sub>3</sub> in NB-PGC units), 3.43 (s, OCH<sub>3</sub> in NB-PGC units), 2.82 (br, CH<sub>2</sub>CH<sub>2</sub> from NHS units), 2.27 (m, CH<sub>2</sub>s from PNB backbone), 1.36–1.27 (m, CH<sub>2</sub>CH<sub>3</sub> in NB-PGC units); <sup>13</sup>C NMR (126 MHz, CDCl<sub>3</sub>)  $\delta$  ppm 154.12, 153.78, 96.34, 77.35, 77.01, 76.71, 73.70, 73.43, 72.75, 66.72, 64.69, 64.60, 55.64, 30.94, 14.12; FT-IR (ATR, cm<sup>-1</sup>) 2982, 1751, 1448, 1373, 1234, 1011, 872, 779. 90% yield.

P(NB-NHS)<sub>157</sub>-*b*-P(NB-*g*-PGC<sub>8</sub>)<sub>12</sub>: <sup>1</sup>H NMR (500 MHz, CDCl<sub>3</sub>)  $\delta$  ppm 5.56 (m, CH=CHs from brush backbone), 5.02 (d, J = 4 Hz, CHOCH<sub>3</sub> in NB-PGC units), 4.26–4.17 (m, OCH<sub>2</sub>CH<sub>3</sub> in NB-PGC units), 3.42 (s, OCH<sub>3</sub> in NB-PGC units), 2.81 (m, CH<sub>2</sub>CH<sub>2</sub> from NHS units), 1.34–1.18 (m, CH<sub>2</sub>CH<sub>3</sub> in NB-PGC units); <sup>13</sup>C NMR (126 MHz, CDCl<sub>3</sub>)  $\delta$  ppm 154.11, 154.10, 153.76, 96.36, 77.30, 77.01, 76.75, 73.69, 73.45, 72.77, 66.71, 64.76, 64.70, 64.58, 55.64, 55.45, 14.10; FT-IR (ATR, cm<sup>-1</sup>) 2981, 1750, 1450, 1373, 1242, 1010, 872, 779. 91% yield.

General Procedure for Hydrolysis of Coil–Brush Block Polymers, P(NB-NHS)-b-P(NB-g-PGC(EC)), Detailed for P(NB-NHS<sub>29</sub>)-b-P(NB-g-PGC<sub>17</sub>)<sub>3</sub>. In a 10 mL Schlenk flask charged with a stir bar, P(NB-g-PGC(EC))-b-P(NB-NHS) (14 mg, 0.80  $\mu$ mol) was dissolved in 5 mL of DMF, and DIPEA (0.010 mL, 7.4 mg, 57  $\mu$ mol) was added into the polymer solution. The reaction was allowed to stir overnight at rt and under nitrogen. After dialysis against nanopure water for 3 days, the product was isolated by lyophilization overnight to give a fluffy white solid (ca. 98% yield).

P(NB-COOH)<sub>54</sub>-b-P(NB-g-PGC<sub>33</sub>)<sub>5</sub>: <sup>1</sup>H NMR (500 MHz, CDCl<sub>3</sub>)  $\delta$  ppm 5.34 (t, J = 9 Hz, CH=CHs from brush backbone), 5.01 (d, J = 4 Hz, CHOCH<sub>3</sub> in NB-PGC units), 4.84 (t, J = 9 Hz, CHOCO in NB-PGC units), 4.72 (m,  $OCH_2CH_3$  in NB-PGC units), 4.19 (m,  $OCH_2CH_3$  in NB-PGC units), 3.42 (s,  $OCH_3$  in NB-PGC units), 2.19 (d, J = 1.0 Hz,  $CH_2$ s from PNB backbone), 1.29 (m,  $CH_2CH_3$  in NB-PGC units); FT-IR (ATR, cm<sup>-1</sup>) 3696–3071, 3071–2808, 1759, 1373, 1250, 1018, 872, 779; DSC  $T_g$  = 93 °C, 116 °C; TGA in Ar 225–322 °C, 58% mass loss.

P(NB-COOH)<sub>89</sub>-b-P(NB-g-PGC<sub>33</sub>)<sub>5</sub>: <sup>1</sup>H NMR (500 MHz, CDCl<sub>3</sub>)  $\delta$  ppm 5.33 (br, CH=CHs from brush backbone), 5.23–5.01 (m, CHOCH<sub>3</sub> in NB-PGC units), 4.82–4.72 ((m, CHOCO in NB-PGC units), 4.32–4.28 (m, OCH<sub>2</sub>CH in NB-PGC units), 4.20–4.19 (m, OCH<sub>2</sub>CH<sub>3</sub> in NB-PGC units), 4.05–4.02 (m, CHCH(CH<sub>2</sub>) O in NB-PGC units), 3.66–3.41 (s, OCH<sub>3</sub> in NB-PGC units), 2.99–2.82 (m, CH<sub>2</sub>s from PNB backbone), 1.29–1.23 (m, CH<sub>2</sub>CH<sub>3</sub> in NB-PGC units); FT-IR (ATR, cm<sup>-1</sup>) 3719–3101, 2970, 1751, 1458,

1366, 1234, 1026, 872, 779; DSC  $T_{\rm g}$  = 95 °C, 152 °C; TGA in Ar 313–360 °C, 60% mass loss.

P(NB-COOH)<sub>26</sub>-b-P(NB-g-PGC<sub>25</sub>)<sub>5</sub>: <sup>1</sup>H NMR (500 MHz, CDCl<sub>3</sub>)  $\delta$  ppm 5.35 (q, J = 9 Hz, CH=CHs from brush backbone), 5.03 (d, J = 4 Hz, CHOCH<sub>3</sub> in NB-PGC units), 4.85 (t, J = 10 Hz, CHOCO in NB-PGC units), 4.74 (d, J = 10 Hz, CHOCH<sub>3</sub> in NB-PGC units), 4.41–4.31 (m,  $OCH_2CH_3$  in NB-PGC units), 4.29–4.21 (m,  $OCH_2CH_3$  in NB-PGC units), 3.47–3.41 (s,  $OCH_3$  in NB-PGC units), 1.40–1.22 (m,  $CH_2CH_3$  in NB-PGC units); FT-IR (ATR, cm<sup>-1</sup>) 3711–2716, 2970, 1751, 1453, 1373, 1250, 1018, 880, 779; DSC  $T_g$  = 93 °C, 125 °C; TGA in Ar 230–350 °C, 55% mass loss.

P(NB-COOH)<sub>59</sub>-b-P(NB-g-PGC<sub>25</sub>)<sub>5</sub>: <sup>1</sup>H NMR (500 MHz, CDCl<sub>3</sub>)  $\delta$  ppm 5.03 (d, J = 4 Hz, CHOCH<sub>3</sub> in NB-PGC units), 4.88–4.81 (m, CHOCO in NB-PGC units), 4.74 (d, J = 10 Hz, CHOCH<sub>3</sub> in NB-PGC units), 4.34 (m, OCH<sub>2</sub>CH<sub>3</sub> in NB-PGC units), 4.26–4.13 (m, OCH<sub>2</sub>CH<sub>3</sub> in NB-PGC units), 3.44 (s, OCH<sub>3</sub> in NB-PGC units), 1.40–1.23 (m, CH<sub>2</sub>CH<sub>3</sub> in NB-PGC units); FT-IR (ATR, cm<sup>-1</sup>) 3742–2731, 2970, 1751, 1628, 1443, 1373, 1242, 1018, 872, 779; DSC  $T_g$  = 94 °C, 126 °C; TGA in Ar 250–355 °C, 53% mass loss.

P(NB-COOH)<sub>29</sub>-b-P(NB-g-PGC<sub>17</sub>)<sub>3</sub>: <sup>1</sup>H NMR (500 MHz, CDCl<sub>3</sub>)  $\delta$  ppm 5.36 (m, CH=CHs from brush backbone), 5.03 (m, CHOCH<sub>3</sub> in NB-PGC units), 4.85 (m, CHOCO in NB-PGC units), 4.74 (d, J=10 Hz, CHOCH<sub>3</sub> in NB-PGC units), 4.33 (m, OCH<sub>2</sub>CH<sub>3</sub> in NB-PGC units), 4.25–4.18 (m, OCH<sub>2</sub>CH<sub>3</sub> in NB-PGC units), 3.50 (s, OCH<sub>3</sub> in NB-PGC units), 1.36–1.26 (m, CH<sub>2</sub>CH<sub>3</sub> in NB-PGC units); FT-IR (ATR, cm<sup>-1</sup>) 3726–3074, 3074–2762, 2970, 1752, 1628, 1250, 1018, 872, 779, 656; DSC  $T_g=90$  °C, 150 °C; TGA in Ar 300–360 °C, 58% mass loss.

P(NB-COOH)<sub>114</sub>-*b*-P(NB-*g*-PGC<sub>17</sub>)<sub>7</sub>: <sup>1</sup>H NMR (500 MHz, CDCl<sub>3</sub>)  $\delta$  ppm 5.32 (br, CH=CHs from brush backbone), 5.02–4.95 (m, CHOCH<sub>3</sub> in NB-PGC units), 4.82–4.68 (m, CHOCO in NB-PGC units), 4.34–4.28 (m, OCH<sub>2</sub>CH in NB-PGC units), 4.22–4.15 (m, OCH<sub>2</sub>CH<sub>3</sub> in NB-PGC units), 4.09–4.02 (m, CHCH(CH<sub>2</sub>) O in NB-PGC units), 3.46–3.37 (s, OCH<sub>3</sub> in NB-PGC units), 2.25–2.02 (m, CH<sub>2</sub>s from PNB backbone), 1.35–1.23 (m, CH<sub>2</sub>CH<sub>3</sub> in NB-PGC units); FT-IR (ATR, cm<sup>-1</sup>) 3711–2710, 1751, 1373, 1250, 1018, 871, 779, 640; DSC  $T_g$  = 93 °C, 148 °C; TGA in Ar 267–372 °C, 63% mass loss.

P(NB-COOH)<sub>322</sub>-*b*-P(NB-*g*-PGC<sub>20</sub>)<sub>12</sub>: <sup>1</sup>H NMR (500 MHz, CDCl<sub>3</sub>)  $\delta$  ppm 5.35–5.27 (m, CH=CHs from brush backbone), 5.00 (d, J = 4 Hz, CHOCH<sub>3</sub> in NB-PGC units), 4.81 (t, J = 10 Hz, CHOCO in NB-PGC units), 4.30 (d, J = 12 Hz, OCH<sub>2</sub>CH in NB-PGC units), 4.24–4.12 (m, OCH<sub>2</sub>CH<sub>3</sub> in NB-PGC units), 4.04 (m, CHCH(CH<sub>2</sub>)O in NB-PGC units), 3.43–3.38 (s, OCH<sub>3</sub> in NB-PGC units), 2.19–2.09 (m, CH<sub>2</sub>s from PNB backbone), 1.33–1.23 (m, CH<sub>2</sub>CH<sub>3</sub> in NB-PGC units); FT-IR (ATR, cm<sup>-1</sup>) 3703–3078, 3078–2777, 1743, 1458, 1373, 1242, 1018, 872, 779, 640; DSC  $T_g$  = 93 °C, 115 °C; TGA in Ar 234–363 °C, 76% mass loss.

P(NB-COOH)<sub>173</sub>-*b*-P(NB-*g*-PGC<sub>25</sub>)<sub>5</sub>: <sup>1</sup>H NMR (500 MHz, CDCl<sub>3</sub>)  $\delta$  ppm 5.35 (t, J = 10 Hz, CH=CHs from brush backbone), 5.03 (m,  $CHOCH_3$  in NB-PGC units), 4.84 (t, J = 10 Hz, CHOCO in NB-PGC units), 4.33 (d, J = 12 Hz,  $OCH_2CH$  in NB-PGC units), 4.26–4.16 (m,  $OCH_2CH_3$  in NB-PGC units), 4.06 (m,  $CHCH(CH_2)$  O in NB-PGC units), 3.43 (q, J = 2 Hz,  $OCH_3$  in NB-PGC units), 2.27 (m,  $CH_2$ s from PNB backbone), 1.34–1.18 (m,  $CH_2CH_3$  in NB-PGC units); <sup>13</sup>C NMR (126 MHz,  $CDCl_3$ )  $\delta$  ppm 154.11, 154.09, 153.76, 96.36, 77.26, 77.03, 76.75, 73.69, 73.43, 72.76, 64.76, 64.68; FT-IR (ATR, cm<sup>-1</sup>) 3742–2731, 1744, 1458, 1380, 1250, 1018, 872, 779; DSC  $T_g$  = 95 °C, 126 °C.; TGA in Ar 242–360 °C, 51% mass loss.

P(NB-COOH)<sub>143</sub>-*b*-P(NB-*g*-PGC<sub>33</sub>)<sub>2</sub>: <sup>1</sup>H NMR (500 MHz, CDCl<sub>3</sub>)  $\delta$  ppm 5.33 (d, J = 10 Hz, CH=CHs from brush backbone), 5.01 (d, J = 4 Hz, CHOCH<sub>3</sub> in NB-PGC units), 4.83 (dd, J = 12 Hz, CHOCO in NB-PGC units), 4.32 (d, J = 12 Hz, OCH<sub>2</sub>CH in NB-PGC units), 4.27–4.12 (m, OCH<sub>2</sub>CH<sub>3</sub> in NB-PGC units), 4.06 (dd, J = 11 Hz, m, CHCH(CH<sub>2</sub>)O in NB-PGC units), 3.49 (s, OCH<sub>3</sub> in NB-PGC units), 2.26 (m, CH<sub>2</sub>s from PNB backbone), 1.29–1.17 (m, CH<sub>2</sub>CH<sub>3</sub> in NB-PGC units); FT-IR (ATR, cm<sup>-1</sup>) 3734–2462, 1744,

1450, 1373, 1242, 1011, 872, 779, 640; DSC  $T_{\rm g}$  = 101 °C, 141 °C; TGA in Ar 251–344 °C, 61% mass loss.

P(NB-COOH)<sub>159</sub>-*b*-P(NB-*g*-PGC<sub>18</sub>)<sub>7</sub>: <sup>1</sup>H NMR (500 MHz, CDCl<sub>3</sub>)  $\delta$  ppm 5.33 (d, J = 10 Hz, CH=CHs from brush backbone), 5.04–4.96 (m,  $CHOCH_3$  in NB-PGC units), 4.84 (q, J = 11 Hz, CHOCO in NB-PGC units), 4.31 (m,  $OCH_2CH$  in NB-PGC units), 4.27–4.12 (m,  $OCH_2CH_3$  in NB-PGC units), 4.08–4.02 (m,  $CHCH(CH_2)O$  in NB-PGC units), 3.42 (s,  $OCH_3$  in NB-PGC units), 2.26 (s,  $CH_2$ s from PNB backbone), 1.29 (m,  $CH_2CH_3$  in NB-PGC units); FT-IR (ATR, cm<sup>-1</sup>) 3726–3078, 2974, 1751, 1250, 1018, 779; DSC  $T_g$  = 97 °C, 153 °C; TGA in Ar 260–373 °C, 64% mass loss.

P(NB-COOH)<sub>139</sub>-b-P(NB-g-PGC<sub>17</sub>)<sub>4</sub>: <sup>1</sup>H NMR (500 MHz, CDCl<sub>3</sub>)  $\delta$  ppm 5.57 (m, CH=CHs from brush backbone), 5.03 (d, J = 4 Hz, CHOCH<sub>3</sub> in NB-PGC units), 4.84 (t, J = 10 Hz, CHOCO in NB-PGC units), 4.27–4.13 (m, OCH<sub>2</sub>CH<sub>3</sub> in NB-PGC units), 3.43 (s, OCH<sub>3</sub> in NB-PGC units), 2.27 (m, CH<sub>2</sub>s from PNB backbone), 1.36–1.27 (m, CH<sub>2</sub>CH<sub>3</sub> in NB-PGC units); FT-IR (ATR, cm<sup>-1</sup>) 3749–3093, 2940, 1744, 1234, 1018, 872, 779; DSC  $T_g$  = 95 °C, 144 °C; TGA in Ar 242–352 °C, 64% mass loss.

P(NB-COOH)<sub>157</sub>-*b*-P(NB-*g*-PGC<sub>8</sub>)<sub>12</sub>: <sup>1</sup>H NMR (500 MHz, CDCl<sub>3</sub>)  $\delta$  ppm 5.56 (m, CH=CHs from brush backbone), 5.02 (d, J = 4 Hz, CHOCH<sub>3</sub> in NB-PGC units), 4.26–4.17 (m, OCH<sub>2</sub>CH<sub>3</sub> in NB-PGC units), 3.42 (s, OCH<sub>3</sub> in NB-PGC units), 2.81 (m, CH<sub>2</sub>CH<sub>2</sub> from NHS units), 1.34–1.18 (m, CH<sub>2</sub>CH<sub>3</sub> in NB-PGC units); FT-IR (ATR, cm<sup>-1</sup>) 3750–3078, 2986, 1751, 1373, 1234, 1018, 871, 779; DSC  $T_g$  = 97 °C, 126 °C; TGA in Ar 225–441 °C, 73% mass loss.

Nanostructure Formation by Supramolecular Assembly in Solution. Each polymer sample was dissolved into DMF to give a 1 mg/mL solution, which was then transferred into presoaked dialysis membrane tubing (MWCO ca. 6–8 kDa) and dialyzed against nanopure water for 3 days at rt. The addition of water induced the assembly and stabilized the formed nanostructures.

Intermediate-Resolution Coarse-Grained Model of P(NB-COOH)-b-P(NB-g-PGC) Coil-Brush Block Polymers. To mimic the length and time scales of the experimental assembly in the simulations of the amphiphilic PGC-based coil-brush block polymers, we developed a coarse-grained model that captures the key physical characteristics of the coil-brush block polymer architecture and yet prevents the simulations from being as computationally expensive as atomistic resolution simulations. In our intermediate resolution CG model (*i.e.*, somewhere between atomistic model and coarser bead spring <sup>86,87</sup> models), we used three types of CG beads (B, A, and N) varying in sizes and interaction. Each solvophobic side chain (B) bead (shown in red in Figure S7) represented four glucose-derived polycarbonate repeat units in the solvophobic side chains; the B diameter was set to 1.00d in simulation units, where 1d corresponds to around 2.8 nm based on the approximate length between four repeat units. One norbornene backbone (N) bead (shown in gray in Figure S7) with a diameter 0.25d represents one repeat unit in the polynorbornene backbone. One solvophilic (A) bead (in blue) represents either one, two, or four repeat units in the solvophilic linear polymer coil; these different bead sizes for the solvophilic beads each representing a different number of (solvophilic) norbornene-based repeat units were tested to determine which more accurately captured the excluded volume of the solvophilic coil upon assembly. The A beads representing one, two, or four repeat units had diameters of 0.25d, 0.50d, or 1.00d, respectively. The best choice of solvophilic bead representation is based on how closely the resulting assembled morphologies from simulations match those from experiments. Our results (Figure S17) show that the best representation is one where each solvophilic A bead of diameter 1.00d represented four repeat units in the solvophilic linear polymer coil.

Irrespective of CG bead type, each bead was bonded to its neighboring bead via a harmonic bond potential, with a force constant of 50  $\varepsilon/d^2$  where  $\varepsilon$  is the energy in reduced Lennard-Jones (LJ)<sup>88</sup> units and had an equilibrium bond distance equal to the arithmetic mean of the bonded bead sizes. The A–A, A–B, A–N, and B–N nonbonded interactions were modeled using purely repulsive Weeks–

Chandler—Andersen<sup>89</sup> (WCA) potential, where the values for the WCA parameters  $\varepsilon$  and  $\sigma$  were 1 (in reduced energy units) and the arithmetic mean of the interacting bead sizes, respectively. The cutoff distance was equal to  $2^{1/6}$  multiplied by the  $\sigma$  of the interacting pair. The effect of solvent quality or *solvophobicity*,  $\varepsilon_{\rm BB}$ , was captured implicitly *via* the strength of attraction between the solvophobic side chain B beads, modeled using an LJ interaction potential that was shifted to have a value of 0 at the cutoff distance 2.5*d*. The values of the  $\varepsilon$  and  $\sigma$  parameters were set to  $\varepsilon_{\rm BB}$  and  $1\sigma$ . Increasing the value of  $\varepsilon_{\rm BB}$  indicates a worsening solvent for the solvophobic block.

Simulation of the Self-Assembly of P(NB-COOH)-b-P(NB-g-PGC). The self-assembly of the coil—brush block polymers in implicit solvent was studied using MD simulations in the NVT ensemble using the Nose-Hoover thermostat with the LAMMPS package. 90 In the simulations, the solvophobicity,  $\varepsilon_{\rm BB}$ , of the system (the degree to which the solvent is poor for the solvophobic components) was gradually increased, driving the assembly of the polymers, similar to a gradual change in solvent composition through dialysis in experiments in Figure S8. As the exact solvophobicity corresponding to each solution concentration throughout the dialysis process was unknown, we gradually changed the solvent quality at both the initial 1.0 mg/mL and the final 0.3 mg/mL polymer concentrations (see Figures S17, S18). Since the micelles assembled at a concentration between the initial 1.0 mg/mL and the final 0.3 mg/mL in experiments during dialysis, we expected that the experimental assembled results would lie in between the assembled results between these two simulation regimes.

We created an initial configuration by randomly placing 600 chains in a cubic simulation box larger than the final size we sampled, to prevent overlap between the chains. We simulated that large simulation box at a temperature of  $T^* = 1.0$  and at low solvophobicity  $(\varepsilon_{\rm BB} = 0.055)$  to relax the configuration away from that initial placement. During this stage, we linearly reduced each of the simulation box sides until we achieved the simulation box size that had the desired polymer concentration; this was done over 3 000 000 time steps where each time step corresponded to  $\Delta t = 0.005$  (in reduced time units). After an additional 3 000 000 time steps, to equilibrate at  $\varepsilon_{BB} = 0.055$  in the simulation box at the desired polymer concentration, the solvophobicity was increased in a stepwise fashion,  $\varepsilon_{{\rm BB,i}}=\varepsilon_{{\rm BB,i-1}}+\Delta\varepsilon_{{\rm BB}}$  with  $\Delta\varepsilon_{{\rm BB}}=0.009.$  At each value of  $\varepsilon_{{\rm BB}}$  we run the simulation for 3 000 000 and 10 000 000 time steps for 1.0 and 0.3 mg/mL, respectively. The choice of  $\Delta \varepsilon_{\rm BB}$  and the number of time steps at each  $\varepsilon_{\mathrm{BB}}$  was chosen after extensive testing that ensured the same equilibrium assembly morphologies were sampled and kinetically trapped morphologies were avoided. These tests included doubling the number of time steps at each solvophobicity as well as running replicate simulations for a select few coil-brush polymers to ensure that these tests resulted in the same morphologies irrespective of the number of time steps or the system size. Overall, the simulation procedure was similar to previously reported protocols. 91,9

**Simulation Analyses.** We visualized the simulations using VMD.<sup>93</sup> Additionally, we investigated the changes in the chain conformations during assembly and calculated the packing parameter of the chains within the simulation as a function of solvophobicity,

Packing Parameter. We calculated the packing parameter, p, as

$$p = \frac{V}{l_c A} \tag{1}$$

after visually confirming that the clusters had assembled and did not change with increasing solvophobicity. The volume of the solvophobic block per chain, V, the length of the solvophobic block per chain within the micelle core,  $l_{c}$ , and the interfacial area between the micelle core and corona per chain, A, were calculated after assembly, depicted in Figure S20.

The volume of the solvophobic block per chain, V, was calculated as

$$V = \frac{\sum_{1}^{N_{\rm B}} V_{\rm B} + \sum_{1}^{N_{\rm N}} V_{\rm N}}{0.64} \tag{2}$$

where the first summation term is the total volume of the solvophobic B side chain beads,  $V_{\rm B}$  is the volume of a B bead, and  $N_{\rm B}$  is the number of B beads per chain and the second summation term is the total volume backbone N beads per chain,  $V_{\rm N}$  is the volume of an N bead,  $N_{\rm N}$  is the number of N beads per chain, and 0.64 is the random sphere packing. By dividing the total volume by 0.64, we can account for void volume during random sphere packing of the spherical beads within the micelle core.

The value of  $l_c$  calculated as

$$l_{c} = \left(\frac{1}{N_{\text{chains}}(N_{\text{B}} + N_{\text{N}} - 1)} \sum_{i}^{N_{\text{chains}}} \sum_{j}^{(N_{\text{B}} + N_{\text{N}} - 1)} (\mathbf{r}_{\text{int},i} - \mathbf{r}_{ij})^{2}\right)^{0.5}$$
(3)

is the average distance from the N backbone CG bead sitting at the interface to the rest of the beads in the backbone and solvophobic block of chain i averaged over all chains,  $N_{\text{chains}}$ , in the simulation. For chain i,  $r_{\text{int},i}$  is the position vector of the its N bead sitting at the interface and  $r_{ij}$  is the position vector of another j bead that is B or another N bead;  $N_{\text{B}}$  and  $N_{\text{N}}$  are the number of B and N beads, respectively, in every chain. Determination of  $l_{\text{c}}$  for the coil—brush polymers is not straightforward, as the solvophobic bottlebrush block is unlike a generic linear chain that stretches into the micelle core. Depending on how we chose to determine  $l_{\text{c}}$ , the values of the packing parameter changed, but the qualitative trends between the packing parameters with changing side chain length and A/G ratio remained the same (data not shown).

The solvent accessible surface area  $(SASA)^{94,95}$  was calculated with a solvent probe radius of  $1\sigma$ ; the probe size was chosen to exclude voids in the micelle core, as we desire to quantify the core—corona interface to determine the packing parameter. The green beads in Figure S20 visualize the SASA. The interfacial area per chain

$$A = \frac{\text{SASA}}{N_{\text{chains}}} \tag{4}$$

was then determined by dividing the calculated area, SASA, by the number of chains,  $N_{\rm chains}$ , in the simulation.

**Chain Conformations.** We calculated the average and the probability distribution of the squared radius of gyration,  $R_{\rm g'}^2$  and the squared end to end distance,  $R_{\rm EE}^2$ , of each side chain, the solvophilic block composed of the A beads,  $R_{\rm g,A}^2$ , and solvophobic block composed of the B and N beads,  $R_{\rm g,B}^2$ , of each chain similarly to that previously reported.

## **ASSOCIATED CONTENT**

### S Supporting Information

The Supporting Information is available free of charge on the ACS Publications website at DOI: 10.1021/acsnano.8b08811.

Additional characterization data (PDF)

## **AUTHOR INFORMATION**

#### **Corresponding Authors**

\*E-mail: pochan@udel.edu. \*E-mail: arthij@udel.edu.

\*E-mail: wooley@chem.tamu.edu.

## ORCID ®

Mei Dong: 0000-0002-9862-0296 Lu Su: 0000-0001-8207-756X Hai Wang: 0000-0002-1215-2613 Arthi Jayaraman: 0000-0002-5295-4581 Karen L. Wooley: 0000-0003-4086-384X

**Author Contributions** <sup>⊥</sup>M.D. and M.G.W. contributed equally

#### Notes

The authors declare no competing financial interest.

#### **ACKNOWLEDGMENTS**

We gratefully acknowledge financial support from the National Science Foundation under grant numbers CHE-1610311, DMREF-1629094, DMREF-1629156, and DMR-1507429, and the Welch Foundation through the W. T. Doherty-Welch Chair in Chemistry under grant number A-0001. We thank Mr. Fanglue Wu and Mr. Fangqing Xia (Department of Materials Science & Engineering, Texas A&M University) for their assistance when AFM and DLS instrumentation, respectively, was inoperable. We thank Dr. Hansoo Kim (Microscopy and Imaging Center, Texas A&M University) for the TEM tomography studies. Dr. Guorong Sun and Dr. Yi-Yun Timothy Tsao (Department of Chemistry, Texas A&M University) are acknowledged for helpful discussions. We also acknowledge the support for the simulation work through the use of information technologies resources at the University of Delaware, specifically the Farber high-performance computing resources.

#### **REFERENCES**

- (1) Wooley, K. L. Shell Crosslinked Polymer Assemblies: Nanoscale Constructs Inspired from Biological Systems. *J. Polym. Sci., Part A: Polym. Chem.* **2000**, 38, 1397–1407.
- (2) O'Reilly, R. K.; Hawker, C. J.; Wooley, K. L. Cross-Linked Block Copolymer Micelles: Functional Nanostructures of Great Potential and Versatility. *Chem. Soc. Rev.* **2006**, *35*, 1068–1083.
- (3) Blanazs, A.; Armes, S. P.; Ryan, A. J. Self-Assembled Block Copolymer Aggregates: From Micelles to Vesicles and their Biological Applications. *Macromol. Macromol. Rapid Commun.* **2009**, 30, 267–277.
- (4) Moughton, A. O.; O'Reilly, R. K. Thermally Induced Micelle to Vesicle Morphology Transition for A Charged Chain End Diblock Copolymer. *Chem. Commun.* **2010**, *46*, 1091–1093.
- (5) Ghoroghchian, P. P.; Li, G.; Levine, D. H.; Davis, K. P.; Bates, F. S.; Hammer, D. A.; Therien, M. J. Bioresorbable Vesicles Formed through Spontaneous Self-Assembly of Amphiphilic Poly(ethylene oxide)-block-Polycaprolactone. *Macromolecules* **2006**, *39*, 1673–1675.
- (6) Zhou, J., Liu, J.; Cheng, C. J.; Patel, T. R.; Weller, C. E.; Piepmeier, J. M.; Jiang, Z.; Saltzman, W. M. Biodegradable Poly(amine-co-ester) Terpolymers for Targeted Gene Delivery. *Nat. Mater.* **2012**, *11*, 82–90.
- (7) Fan, J.; Zou, J.; He, X.; Zhang, F.; Zhang, S.; Raymond, J. E.; Wooley, K. L. Tunable Mechano-Responsive Organogels by Ring-Opening Copolymerizations of *N*-carboxyanhydrides. *Chem. Sci.* **2014**, *S*, 141–150.
- (8) Lu, H.; Wang, J.; Song, Z.; Yin, L.; Zhang, Y.; Tang, H.; Tu, C.; Lin, Y.; Cheng, J. Recent Advances in Amino Acid N-Carboxyanhydrides and Synthetic Polypeptides: Chemistry, Self-Assembly and Biological Applications. Chem. Commun. 2014, 50, 139–155.
- (9) Zhang, F.; Zhang, S.; Pollack, S. F.; Li, R.; Gonzalez, A. M.; Fan, J.; Zou, J.; Leininger, S. E.; Pavía-Sanders, A.; Johnson, R.; Nelson, L. D.; Raymond, J. E.; Elsabahy, M.; Hughes, D. M. P.; Lenox, M. W.; Gustafson, T. P.; Wooley, K. L. Improving Paclitaxel Delivery: *In Vitro* and *In Vivo* Characterization of PEGylated Polyphosphoester-Based Nanocarriers. *J. Am. Chem. Soc.* 2015, 137, 2056–2066.
- (10) Song, Y.; Chen, Y.; Su, L.; Li, R.; Letteri, R. A.; Wooley, K. L. Crystallization-Driven Assembly of Fully Degradable, Natural Product-Based Poly(L-lactide)-block-Poly( $\alpha$ -D-glucose carbonate)s in Aqueous Solution. *Polymer* **2017**, 122, 270–279.
- (11) Su, L.; Khan, S.; Fan, J.; Lin, Y.-N.; Wang, H.; Gustafson, T. P.; Zhang, F.; Wooley, K. L. Functional Sugar-Based Polymers and Nanostructures Comprised of Degradable Poly(D-glucose carbonate)s. *Polym. Chem.* **2017**, *8*, 1699–1707.

(12) Lin, Y.-N.; Su, L.; Smolen, J.; Li, R.; Song, Y.; Wang, H.; Dong, M.; Wooley, K. L. Co-Assembly of Sugar-Based Amphiphilic Block Polymers to Achieve Nanoparticles with Tunable Morphology, Size, Surface Charge, and Acid-Responsive Behavior. *Mater. Chem. Front.* **2018**, *2*, 2230–2238.

- (13) Osumi, S.; Felder, S. E.; Wang, H.; Lin, Y.-N.; Dong, M.; Wooley, K. L. Construction of Nanostructures in Aqueous Solution from Amphiphilic Glucose-Derived Polycarbonates. *J. Polym. Sci., Part A: Polym. Chem.* **2019**, *57*, 432–440.
- (14) Du, J.-Z.; Tang, L.-Y.; Song, W.-J.; Shi, Y.; Wang, J. Evaluation of Polymeric Micelles from Brush Polymer with Poly( $\varepsilon$ -caprolactone)-b-Poly(ethylene glycol) Side Chains as Drug Carrier. Biomacromolecules **2009**, 10, 2169–2174.
- (15) Nasongkla, N.; Chen, B.; Macaraeg, N.; Fox, M. E.; Fréchet, J. M. J.; Szoka, F. C. Dependence of Pharmacokinetics and Biodistribution on Polymer Architecture: Effect of Cyclic *versus* Linear Polymers. J. Am. Chem. Soc. 2009, 131, 3842–3843.
- (16) Voit, B. I.; Lederer, A. Hyperbranched and Highly Branched Polymer Architectures-Synthetic Strategies and Major Characterization Aspects. *Chem. Rev.* **2009**, *109*, 5924–5973.
- (17) Rzayev, J. Molecular Bottlebrushes: New Opportunities in Nanomaterials Fabrication. ACS Macro Lett. 2012, 1, 1146–1149.
- (18) Verduzco, R.; Li, X.; Pesek, S. L.; Stein, G. E. Structure, Function, Self-Assembly, and Applications of Bottlebrush Copolymers. *Chem. Soc. Rev.* **2015**, *44*, 2405–2420.
- (19) Müllner, M.; Müller, A. H. E. Cylindrical Polymer Brushes Anisotropic Building Blocks, Unimolecular Templates and Particulate Nanocarriers. *Polymer* **2016**, *98*, 389–401.
- (20) Lu, S.; Seong, H. G.; Yen-Nan, L.; Mei, D.; Shiyi, Z.; Yingchao, C.; Guorong, S.; Wooley, K. L. Syntheses of Triblock Bottlebrush Polymers Through Sequential ROMPs: Expanding the Functionalities of Molecular Brushes. *J. Polym. Sci., Part A: Polym. Chem.* **2017**, *55*, 2966–2970.
- (21) Fu, G. D.; Phua, S. J.; Kang, E. T.; Neoh, K. G. Tadpole-Shaped Amphiphilic Block—Graft Copolymers Prepared *via* Consecutive Atom Transfer Radical Polymerizations. *Macromolecules* **2005**, 38, 2612–2619.
- (22) Olsen, B. D.; Segalman, R. A. Structure and Thermodynamics of Weakly Segregated Rod-Coil Block Copolymers. *Macromolecules* **2005**, 38, 10127–10137.
- (23) Du, J.-Z.; Chen, D.-P.; Wang, Y.-C.; Xiao, C.-S.; Lu, Y.-J.; Wang, J.; Zhang, G.-Z. Synthesis and Micellization of Amphiphilic Brush—Coil Block Copolymer Based on Poly( $\varepsilon$ -caprolactone) and PEGylated Polyphosphoester. *Biomacromolecules* **2006**, *7*, 1898—1903.
- (24) Bernaerts, K. V.; Fustin, C.-A.; Bomal-D'Haese, C.; Gohy, J.-F.; Martins, J. C.; Du Prez, F. E. Advanced Polymer Architectures with Stimuli-Responsive Properties Starting from Inimers. *Macromolecules* **2008**, *41*, 2593–2606.
- (25) Ishizu, K.; Hatoyama, N.; Uchida, S. Architecture of Rod-Brush Block Copolymers Synthesized by A Combination of Coordination Polymerization and Atom Transfer Radical Polymerization. *J. Appl. Polym. Sci.* **2008**, *108*, 3346–3352.
- (26) Tao, Y.; Ma, B.; Segalman, R. A. Self-Assembly of Rod—Coil Block Copolymers and Their Application in Electroluminescent Devices. *Macromolecules* **2008**, *41*, 7152—7159.
- (27) Feng, C.; Shen, Z.; Li, Y.; Gu, L.; Zhang, Y.; Lu, G.; Huang, X. PNIPAM-b-(PEA-g-PDMAEA) Double-Hydrophilic Graft Copolymer: Synthesis and Its Application for Preparation of Gold Nanoparticles in Aqueous Media. *J. Polym. Sci., Part A: Polym. Chem.* 2009, 47, 1811–1824.
- (28) Li, C.; Ge, Z.; Fang, J.; Liu, S. Synthesis and Self-Assembly of Coil—Rod Double Hydrophilic Diblock Copolymer with Dually Responsive Asymmetric Centipede-Shaped Polymer Brush as the Rod Segment. *Macromolecules* **2009**, *42*, 2916—2924.
- (29) Sun, R.; Wang, G.; Liu, C.; Huang, J. Preparation of Comb-Like Copolymers with Amphiphilic Poly(ethylene oxide)-b-Polystyrene Graft Chains by Combination of "Graft From" and "Graft Onto" Strategies. J. Polym. Sci., Part A: Polym. Chem. 2009, 47, 1930–1938.

(30) Wang, W.; Liu, R.; Li, Z.; Meng, C.; Wu, Q.; Zhu, F. Synthesis and Self-Assembly of New Double-Crystalline Amphiphilic Polyethylene-block-Poly[oligo(ethylene glycol) Methyl Ether Methacrylate] Coil-Brush Diblock Copolymer. *Macromol. Chem. Phys.* **2010**, 211, 1452–1459.

- (31) Banquy, X.; Burdyńska, J.; Lee, D. W.; Matyjaszewski, K.; Israelachvili, J. Bioinspired Bottle-Brush Polymer Exhibits Low Friction and Amontons-Like Behavior. *J. Am. Chem. Soc.* **2014**, *136*, 6199–6202.
- (32) Jonikaite-Svegzdiene, J.; Kudresova, A.; Paukstis, S.; Skapas, M.; Makuska, R. Synthesis and Self-Assembly of Polystyrene-Based Diblock and Triblock Coil-Brush Copolymers. *Polym. Chem.* **2017**, 8, 5621–5632.
- (33) Riess, G. Micellization of Block Copolymers. *Prog. Polym. Sci.* **2003**, 28, 1107–1170.
- (34) Hadjichristidis, N.; Iatrou, H.; Pitsikalis, M.; Pispas, S.; Avgeropoulos, A. Linear and Non-Linear Triblock Terpolymers. Synthesis, Self-Assembly in Selective Solvents and in Bulk. *Prog. Polym. Sci.* **2005**, *30*, 725–782.
- (35) Rodríguez-Hernández, J.; Chécot, F.; Gnanou, Y.; Lecommandoux, S. Toward 'Smart' Nano-Objects by Self-Assembly of Block Copolymers in Solution. *Prog. Polym. Sci.* **2005**, *30*, 691–724.
- (36) Ruokolainen, J.; Saariaho, M.; Ikkala, O.; ten Brinke, G.; Thomas, E. L.; Torkkeli, M.; Serimaa, R. Supramolecular Routes to Hierarchical Structures: Comb-Coil Diblock Copolymers Organized with Two Length Scales. *Macromolecules* 1999, 32, 1152–1158.
- (37) Xu, X.; Jia, Z.; Sun, R.; Huang, J. Synthesis of Well-Defined, Brush-Type, Amphiphilic [Poly(styrene-co-2-hydroxyethyl methacrylate)-graft-Poly( $\varepsilon$ -caprolactone)]-b-Poly(ethylene oxide)-b-[Poly(styrene-co-2-hydroxyethyl methacrylate)-graft-Poly( $\varepsilon$ -caprolactone)] and Its Aggregation Behavior in Aqueous Media. J. Polym. Sci., Part A: Polym. Chem. 2006, 44, 4396–4408.
- (38) Bougard, F.; Giacomelli, C.; Mespouille, L.; Borsali, R.; Dubois, P.; Lazzaroni, R. Influence of the Macromolecular Architecture on the Self-Assembly of Amphiphilic Copolymers Based on Poly(N,N-dimethylamino-2-ethyl methacrylate) and Poly( $\varepsilon$ -caprolactone). Langmuir 2008, 24, 8272–8279.
- (39) Qi, H.; Zhong, C. Density Functional Theory Studies on the Microphase Separation of Amphiphilic Comb Copolymers in a Selective Solvent. *J. Phys. Chem. B* **2008**, *112*, 10841–10847.
- (40) Khelfallah, N.; Gunari, N.; Fischer, K.; Gkogkas, G.; Hadjichristidis, N.; Schmidt, M. Micelles Formed by Cylindrical Brush-Coil Block Copolymers. *Macromol. Rapid Commun.* **2005**, 26, 1693—1697
- (41) Zamurovic, M.; Christodoulou, S.; Vazaios, A.; Iatrou, E.; Pitsikalis, M.; Hadjichristidis, N. Micellization Behavior of Complex Comblike Block Copolymer Architectures. *Macromolecules* **2007**, *40*, 5835–5849.
- (42) Yi, Z.; Liu, X.; Jiao, Q.; Chen, E.; Chen, Y.; Xi, F. Synthesis, Characterization, and Self-Assembly of Comb-Dendronized Amphiphilic Block Copolymers. *J. Polym. Sci., Part A: Polym. Chem.* **2008**, 46, 4205–4217.
- (43) Cai, C.; Zhu, W.; Chen, T.; Lin, J.; Tian, X. Synthesis and Self-Assembly Behavior of Amphiphilic Polypeptide-Based Brush-Coil Block Copolymers. *J. Polym. Sci., Part A: Polym. Chem.* **2009**, 47, 5967–5978.
- (44) Zhulina, E. B.; Adam, M.; LaRue, I.; Sheiko, S. S.; Rubinstein, M. Diblock Copolymer Micelles in a Dilute Solution. *Macromolecules* **2005**, 38, 5330–5351.
- (45) Wu, W.-C.; Tian, Y.; Chen, C.-Y.; Lee, C.-S.; Sheng, Y.-J.; Chen, W.-C.; Alex, K.-Y. J. Theoretical and Experimental Studies on the Surface Structures of Conjugated Rod—Coil Block Copolymer Brushes. *Langmuir* **2007**, *23*, 2805—2814.
- (46) Percec, V.; Wilson, D. A.; Leowanawat, P.; Wilson, C. J.; Hughes, A. D.; Kaucher, M. S.; Hammer, D. A.; Levine, D. H.; Kim, A. J.; Bates, F. S. Self-Assembly of Janus Dendrimers into Uniform Dendrimersomes and Other Complex Architectures. *Science* **2010**, 328, 1009–1014.

- (47) Zhuang, Z.; Zhu, X.; Cai, C.; Lin, J.; Wang, L. Self-Assembly of a Mixture System Containing Polypeptide Graft and Block Copolymers: Experimental Studies and Self-Consistent Field Theory Simulations. *J. Phys. Chem. B* **2012**, *116*, 10125–10134.
- (48) Zhulina, E.; Borisov, O. Theory of Block Polymer Micelles: Recent Advances and Current Challenges. *Macromolecules* **2012**, *45*, 4429–4440.
- (49) Cai, C.; Li, Y.; Lin, J.; Wang, L.; Lin, S.; Wang, X. S.; Jiang, T. Simulation-Assisted Self-Assembly of Multicomponent Polymers into Hierarchical Assemblies with Varied Morphologies. *Angew. Chem.* **2013**, *125*, 7886–7890.
- (50) Gu, W.; Huh, J.; Hong, S. W.; Sveinbjornsson, B. R.; Park, C.; Grubbs, R. H.; Russell, T. P. Self-Assembly of Symmetric Brush Diblock Copolymers. *ACS Nano* **2013**, *7*, 2551–2558.
- (51) Dalsin, S. J.; Rions-Maehren, T. G.; Beam, M. D.; Bates, F. S.; Hillmyer, M. A.; Matsen, M. W. Bottlebrush Block Polymers: Quantitative Theory and Experiments. *ACS Nano* **2015**, *9*, 12233–12245.
- (52) Li, N. K.; Fuss, W. H.; Tang, L.; Gu, R.; Chilkoti, A.; Zauscher, S.; Yingling, Y. G. Prediction of Solvent-Induced Morphological Changes of Polyelectrolyte Diblock Copolymer Micelles. *Soft Matter* **2015**, *11*, 8236–8245.
- (53) Li, Y.; Jiang, T.; Lin, S.; Lin, J.; Cai, C.; Zhu, X. Hierarchical Nanostructures Self-Assembled from a Mixture System Containing Rod-Coil Block Copolymers and Rigid Homopolymers. *Sci. Rep.* **2015**, *5*, 10137.
- (54) Zhang, Q.; Lin, J.; Wang, L.; Xu, Z. Theoretical Modeling and Simulations of Self-Assembly of Copolymers in Solution. *Prog. Polym. Sci.* **2017**, *75*, 1–30.
- (55) Alaboalirat, M.; Qi, L.; Arrington, K. J.; Qian, S.; Keum, J. K.; Mei, H.; Littrell, K. C.; Sumpter, B. G.; Carrillo, J.-M. Y.; Verduzco, R.; Matson, J. B. Amphiphilic Bottlebrush Block Copolymers: Analysis of Aqueous Self-Assembly by Small-Angle Neutron Scattering and Surface Tension Measurements. *Macromolecules* 2019, 52, 465–476.
- (56) Ianiro, A.; Wu, H.; van Rijt, M. M. J.; Vena, M. P.; Keizer, A. D. A.; Esteves, A. C. C.; Tuinier, R.; Friedrich, H.; Sommerdijk, N. A. J. M.; Patterson, J. P. Liquid—Liquid Phase Separation During Amphiphilic Self-Assembly. *Nat. Chem.* **2019**, *11*, 320—328.
- (57) Vasilevskaya, V.; Gusev, L.; Khokhlov, A.; Ikkala, O.; Ten Brinke, G. Domains in Melts of Comb-Coil Diblock Copolymers: Superstrong Segregation Regime. *Macromolecules* **2001**, *34*, 5019–5022.
- (58) Nap, R. J.; Ten Brinke, G. Ordering at Two Length Scales in Comb—Coil Diblock Copolymers Consisting of Only Two Different Monomers. *Macromolecules* **2002**, *35*, 952—959.
- (59) Huang, C. I.; Lin, Y. C. Hierarchical Structure-within-Structure Morphologies in A-block-(B-graft-C) Molecules. *Macromol. Rapid Commun.* **2007**, 28, 1634–1639.
- (60) Huang, C.-I. Self-Assembling of Block Copolymers Involving Competing Length Scales. *React. Funct. Polym.* **2009**, *69*, 530–538.
- (61) Wang, L.; Lin, J.; Zhang, L. Hierarchically Ordered Microstructures Self-Assembled from Comb-Coil Block Copolymers. *Langmuir* **2009**, 25, 4735–4742.
- (62) Wang, L.; Lin, J.; Zhang, L. Hierarchically Ordered Microstructures Self-Assembled from A (BC) n Multiblock Copolymers. *Macromolecules* **2010**, 43, 1602–1609.
- (63) Wang, R.; Jiang, Z.; Yang, H.; Xue, G. Side Chain Effect on the Self-Assembly of Coil-Comb Copolymer by Self-Consistent Field Theory in Two Dimensions. *Polymer* **2013**, *54*, 7080–7087.
- (64) Jiang, Z.; Qian, Z.; Yang, H.; Wang, R. Disorder to Order Transition and Ordered Morphology of Coil-Comb Block Copolymer by Self-Consistent Field Theory. *Nanoscale Res. Lett.* **2015**, *10*, 328.
- (65) Wood, K. C.; Little, S. R.; Langer, R.; Hammond, P. T. A Family of Hierarchically Self-Assembling Linear-Dendritic Hybrid Polymers for Highly Efficient Targeted Gene Delivery. *Angew. Chem., Int. Ed.* **2005**, 44, 6704–6708.
- (66) Cheng, L.; Cao, D. Effect of Tail Architecture on Self-Assembly of Amphiphiles for Polymeric Micelles. *Langmuir* **2009**, *25*, 2749–2756.

(67) Wang, J.; Guo, K.; An, L.; Muller, M.; Wang, Z.-G. Micelles of Coil-Comb Block Copolymers in Selective Solvents: Competition of Length Scales. *Macromolecules* **2010**, *43*, 2037–2041.

- (68) Lin, Y.-L.; Chang, H.-Y.; Sheng, Y.-J.; Tsao, H.-K. Photoresponsive Polymersomes Formed by Amphiphilic Linear—Dendritic Block Copolymers: Generation-Dependent Aggregation Behavior. *Macromolecules* **2012**, *45*, 7143—7156.
- (69) Liu, Y.; Zhang, Y.; Wang, Z.; Wang, J.; Wei, K.; Chen, G.; Jiang, M. Building Nanowires from Micelles: Hierarchical Self-Assembly of Alternating Amphiphilic Glycopolypeptide Brushes with Pendants of High-Mannose Glycodendron and Oligophenylalanine. *J. Am. Chem. Soc.* 2016, 138, 12387–12394.
- (70) Yu, W.; Inam, M.; Jones, J. R.; Dove, A. P.; O'Reilly, R. K. Understanding the CDSA of Poly(lactide) Containing Triblock Copolymers. *Polym. Chem.* **2017**, *8*, 5504–5512.
- (71) Israelachvili, J. N.; Mitchell, D. J.; Ninham, B. W. Theory of Self-Assembly of Hydrocarbon Amphiphiles into Micelles and Bilayers. *J. Chem. Soc., Faraday Trans.* 2 **1976**, 72, 1525–1568.
- (72) Samarajeewa, S.; Shrestha, R.; Li, Y.; Wooley, K. L. Degradability of Poly(Lactic Acid)-Containing Nanoparticles: Enzymatic Access through a Cross-Linked Shell Barrier. *J. Am. Chem. Soc.* **2012**, *134*, 1235–1242.
- (73) Gregory, G. L.; Jenisch, L. M.; Charles, B.; Kociok-Köhn, G.; Buchard, A. Polymers from Sugars and CO<sub>2</sub>: Synthesis and Polymerization of a D-Mannose-Based Cyclic Carbonate. *Macromolecules* **2016**, 49, 7165–7169.
- (74) Tanner, P.; Baumann, P.; Enea, R.; Onaca, O.; Palivan, C.; Meier, W. Polymeric Vesicles: From Drug Carriers to Nanoreactors and Artificial Organelles. *Acc. Chem. Res.* **2011**, *44*, 1039–1049.
- (75) Geng, Y.; Dalhaimer, P.; Cai, S.; Tsai, R.; Tewari, M.; Minko, T.; Discher, D. E. Shape Effects of Filaments *versus* Spherical Particles in Flow and Drug Delivery. *Nat. Nanotechnol.* **2007**, *2*, 249.
- (76) Gratton, S. E. A.; Ropp, P. A.; Pohlhaus, P. D.; Luft, J. C.; Madden, V. J.; Napier, M. E.; DeSimone, J. M. The Effect of Particle Design on Cellular Internalization Pathways. *Proc. Natl. Acad. Sci. U. S. A.* 2008, 105, 11613–11618.
- (77) Albanese, A.; Tang, P. S.; Chan, W. C. W. The Effect of Nanoparticle Size, Shape, and Surface Chemistry on Biological Systems. *Annu. Rev. Biomed. Eng.* **2012**, *14*, 1–16.
- (78) Unsal, H.; Onbulak, S.; Calik, F.; Er-Rafik, M.; Schmutz, M.; Sanyal, A.; Rzayev, J. Interplay Between Molecular Packing, Drug Loading, and Core Cross-Linking in Bottlebrush Copolymer Micelles. *Macromolecules* **2017**, *50*, 1342–1352.
- (79) Miller, S. A. Sustainable Polymers: Opportunities for the Next Decade. *ACS Macro Lett.* **2013**, *2*, 550–554.
- (80) Zhu, Y.; Romain, C.; Williams, C. K. Sustainable Polymers from Renewable Resources. *Nature* **2016**, *540*, 354–362.
- (81) Hillmyer, M. A. The Promise of Plastics from Plants. *Science* **2017**, 358, 868–870.
- (82) De Hoe, G. X.; Zumstein, M. T.; Tiegs, B. J.; Brutman, J. P.; McNeill, K.; Sander, M.; Coates, G. W.; Hillmyer, M. A. Sustainable Polyester Elastomers from Lactones: Synthesis, Properties, and Enzymatic Hydrolyzability. J. Am. Chem. Soc. 2018, 140, 963–973.
- (83) Song, Y.; Ji, X.; Dong, M.; Li, R.; Lin, Y.-N.; Wang, H.; Wooley, K. L. Advancing the Development of Highly-Functionalizable Glucose-Based Polycarbonates by Tuning of the Glass Transition Temperature. J. Am. Chem. Soc. 2018, 140, 16053–16057.
- (84) Wang, H.; Dong, M.; Khan, S.; Su, L.; Li, R.; Song, Y.; Lin, Y.-N.; Kang, N.; Komatsu, C. H.; Elsabahy, M.; Wooley, K. L. Acid-Triggered Polymer Backbone Degradation and Disassembly to Achieve Release of Camptothecin from Functional Polyphosphoramidate Nanoparticles. ACS Macro Lett. 2018, 7, 783–788.
- (85) Choi, T.-L.; Grubbs, R. H. Controlled Living Ring-Opening-Metathesis Polymerization by a Fast-Initiating Ruthenium Catalyst. *Angew. Chem., Int. Ed.* **2003**, 42, 1743–1746.
- (86) Ceperley, D.; Kalos, M.; Lebowitz, J. L. Computer Simulation of the Dynamics of a Single Polymer Chain. *Phys. Rev. Lett.* **1978**, 41, 313–316.

(87) Grest, G. S.; Kremer, K. Molecular Dynamics Simulation for Polymers in the Presence of a Heat Bath. *Phys. Rev. A: At., Mol., Opt. Phys.* **1986**, 33, 3628–3631.

- (88) Jones, J. E. On the Determination of Molecular Fields.—I. From the Variation of the Viscosity of a Gas with Temperature. *Proc. R. Soc. London, Ser. A* **1924**, *106*, 441–462.
- (89) Weeks, J. D.; Chandler, D.; Andersen, H. C. Role of Repulsive Forces in Determining the Equilibrium Structure of Simple Liquids. *J. Chem. Phys.* **1971**, *54*, 5237–5247.
- (90) Plimpton, S. Fast Parallel Algorithms for Short-Range Molecular Dynamics. *J. Comput. Phys.* **1995**, *117*, 1–19.
- (91) Lyubimov, I.; Beltran-Villegas, D. J.; Jayaraman, A. PRISM Theory Study of Amphiphilic Block Copolymer Solutions with Varying Copolymer Sequence and Composition. *Macromolecules* **2017**, *50*, 7419–7431.
- (92) Beltran-Villegas, D. J.; Jayaraman, A. Assembly of Amphiphilic Block Copolymers and Nanoparticles in Solution: Coarse-Grained Molecular Simulation Study. *J. Chem. Eng. Data* **2018**, *63*, 2351–2367.
- (93) Humphrey, W.; Dalke, A.; Schulten, K. VMD: Visual Molecular Dynamics. *J. Mol. Graphics* **1996**, *14*, 33–38.
- (94) Lee, B.; Richards, F. M. The Interpretation of Protein Structures: Estimation of Static Accessibility. *J. Mol. Biol.* **1971**, *55*, 379–IN4.
- (95) Shrake, A.; Rupley, J. Environment and Exposure to Solvent of Protein Atoms. Lysozyme and Insulin. *J. Mol. Biol.* **1973**, *79*, 351–371.
- (96) Lin, B.; Martin, T. B.; Jayaraman, A. Decreasing Polymer Flexibility Improves Wetting and Dispersion of Polymer-Grafted Particles in a Chemically Identical Polymer Matrix. *ACS Macro Lett.* **2014**, *3*, 628–632.